BOREAS An international journal of Quaternary research

Holocene variability in sea-ice conditions in the eastern Baffin Bay-Labrador Sea – A north–south biomarker transect study

JEETENDRA SAINI, RUEDIGER STEIN, KIRSTEN FAHL, JENS WEISER, DIERK HEBBELN AND LINA MADAJ

BOREAS

Saini, J., Stein, R., Fahl, K., Weiser, J., Hebbeln, D. & Madaj, L. 2022 (July): Holocene variability in sea-ice conditions in the eastern Baffin Bay-Labrador Sea – A north–south biomarker transect study. *Boreas*, Vol. 51, pp. 553–572. https://doi.org/10.1111/bor.12583. ISSN 0300-9483.

Reconstructions of sea-surface conditions during the Holocene were achieved using three sediment cores from northeastern Baffin Bay (GeoB19948-3 and GeoB19927-3) and the Labrador Sea (GeoB19905-1) along a north–south transect based on sea-ice IP_{25} and open-water phytoplankton biomarkers (brassicasterol, dinosterol and HBI III). In Baffin Bay, sea-surface conditions in the Early Holocene were characterized by extended (early) spring sea ice cover (SIC) prior to 7.6 ka BP. The conditions in the NE Labrador Sea, however, remained predominantly ice-free in spring/autumn due to the enhanced influx of Atlantic Water (West Greenland Current, WGC) from 11.5 until ~9.1 ka BP, succeeded by a period of continued (spring–autumn) ice-free conditions between 9.1 and 7.6 ka BP corresponding to the onset of Holocene Thermal Maximum (HTM)-like conditions. A transition towards reoccurring ice-edge and significantly reduced SIC conditions in Baffin Bay is evident in the Middle Holocene (~7.6–3 ka BP) probably caused by the variations in the WGC influence associated with the ice melting and can be characterized as HTM-like conditions. These HTM-like conditions are predominantly recorded in the NE Labrador Sea area shown by (spring–autumn) ice-free conditions from 5.9–3 ka BP. In the Late Holocene (last ~3 ka), our combined proxy records from eastern Baffin Bay indicate low *in-situ* ice algae production; however, enhanced multi-year (drifted) sea ice in this area was possibly attributed to the increased influx of Polar Water mass influx and may correlate with the Neoglacial cooling. The conditions in the NE Labrador Sea during the last 3 ka, however, continued to remain (spring–autumn) ice-free. Our data from the Baffin Bay–Labrador Sea transect suggest a dominant influence of meltwater influx on sea-ice formation throughout the Holocene, in contrast to sea-ice records from the Fram Strait area, which seem to follow predominantly the summer insolation trend.

Jeetendra Saini (jeetendra077@gmail.com) and Kirsten Fahl, Alfred-Wegener-Institute, Helmholtz Centre for Polar and Marine Research, Am Alten Hafen 26, 27568 Bremerhaven, Germany; Ruediger Stein, Alfred-Wegener-Institute, Helmholtz Centre for Polar and Marine Research, Am Alten Hafen 26, 27568 Bremerhaven, Germany and MARUM-Center for Marine Environmental Sciences, University of Bremen, Leobener Str. 8, 28359 Bremen, Germany; Jens Weiser, Dierk Hebbeln and Lina Madaj, MARUM-Center for Marine Environmental Sciences, University of Bremen, Leobener Str. 8, 28359 Bremen, Germany; *received 26th March 2021, accepted 29th December 2021.*

Sea ice with its strong seasonal and interannual variability plays a fundamental role in the Earth's climate system as it influences the heat, moisture, albedo and gas exchange between the ocean and the atmosphere as well as deep-water formation (Dieckmann & Hellmer 2003; McPhee *et al.* 2009; Thomas & Dieckmann 2010; Morison *et al.* 2012). Over the last few decades, the Arctic sea ice has undergone a considerable reduction in its extent and thickness due to modern climate warming (Kinnard *et al.* 2011; Serreze & Stroeve 2015; NSIDC 2020) and indeed this has raised considerable concerns about sea-ice variability in the future (Bhatt *et al.* 2014). It is expected that this ongoing reduction of Arctic sea ice will continue and amplify, further decreasing the Arctic Ocean albedo thus increasing sea-surface temperatures (SSTs; Manabe *et al.* 1992; Screen & Simmonds 2010). To understand these rapid changes in sea ice cover from a long-term perspective, there is a need for a better understanding of the sea-ice variability as well as its dynamics and interaction with climate throughout the geological past (Jakobsson *et al.* 2010).

Various proxies preserved in marine sediments may indicate indirect changes in sea-ice occurrence and variability, as inferred from micropalaeontology (e.g. dinoflagellate cysts, diatoms, and foraminifera assemblages) (Jennings *et al.* 2002; Gersonde *et al.* 2005; de Vernal *et al.* 2013a, b), geochemistry (Hillaire-Marcel & de Vernal 2008) and sedimentology (e.g. ice-rafted debris; Polyak *et al.* 2010). The biomarker proxy 'IP_{25}', exclusively synthesized by sea-ice algae and well preserved in the sediments, however, seems to be a direct indicator for the presence of seasonal Arctic sea ice as shown in the pioneer study by Belt *et al.* (2007) (see Belt 2018 for a recent review). Even more detailed and semi-quantitative reconstructions of sea ice cover can be obtained when combining IP_{25} with open-water phytoplankton biomarkers such as brassicasterol, dinosterol and/or a highly branched unsaturated triene (HBI III) ('PIP_{25} index' Müller *et al.* 2011; Belt *et al.* 2015, 2019; Smik *et al.* 2016).

Arctic outflow through Baffin Bay, via the Labrador Sea, acts as a substantial contributor of fresh water to the North Atlantic, as suggested by modelling and observational studies (Bunker 1976; Tang *et al.* 2004; Serreze *et al.* 2006; Aksenov *et al.* 2010). Baffin Bay is characterized by a sea ice cover during most time of the year; however, further to the south, the eastern Labrador Sea is predominantly ice-free (Tang *et al.* 2004). Thus the Baffin

DOI 10.1111/bor.12583

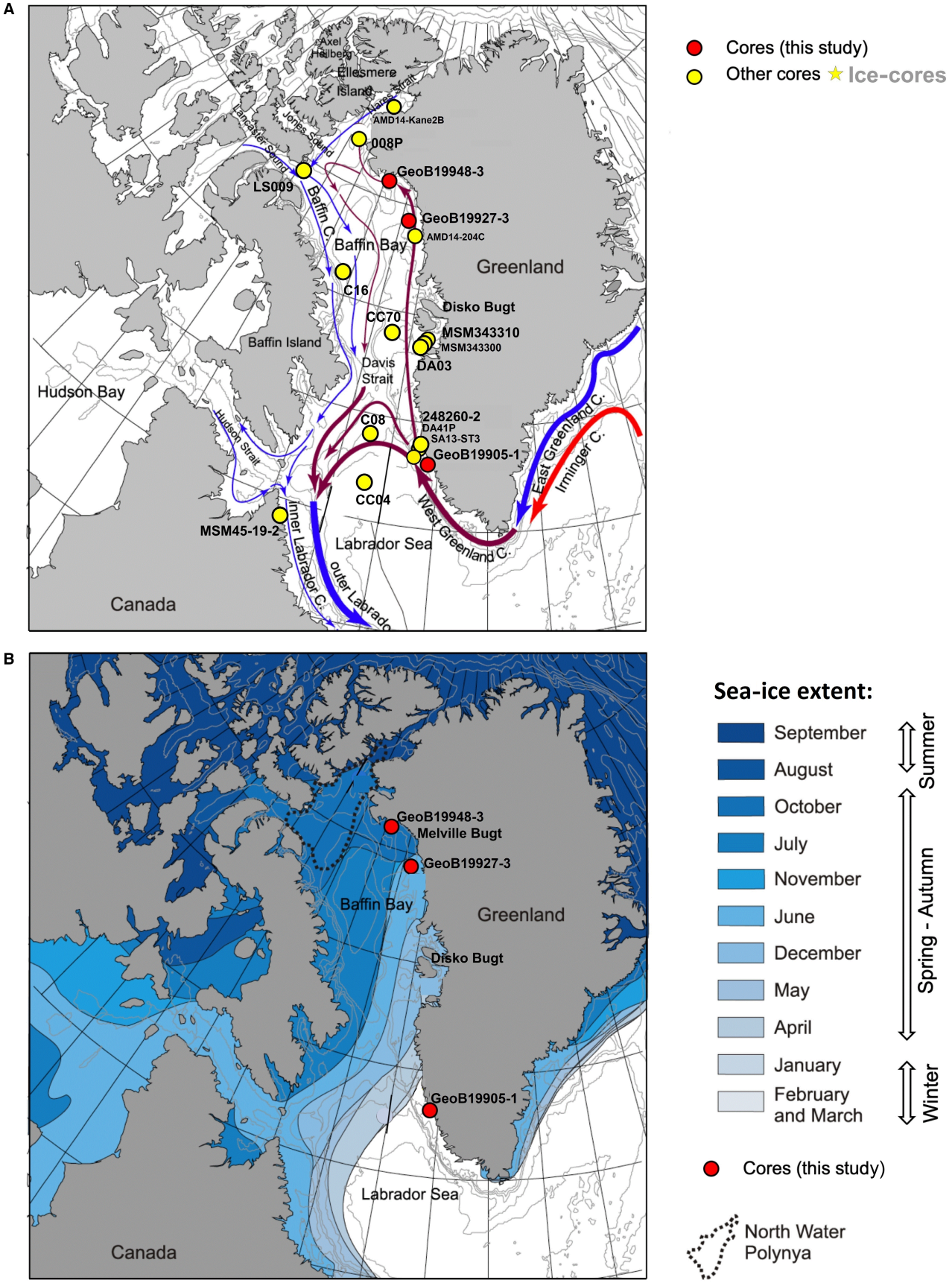
A
Axel Heiberg
Ellesmere Island
Nares Strait
AMD14-Kane2B
008P
Lancaster Sound
Jones Sound
LS009
Baffin C.
GeoB19948-3
GeoB19927-3
AMD14-204C
Baffin Bay
Greenland
C16
Disko Bugt
CC70
MSM343310
MSM343300
Baffin Island
DA03
Davis Strait
Hudson Bay
Hudson Strait
C08
248260-2
DA41P
SA13-ST3
GeoB19905-1
East Greenland C.
Irminger C.
CC04
West Greenland C.
MSM45-19-2
Inner Labrador C.
Labrador Sea
outer Labrado
Canada
Cores (this study)
Other cores
Ice-cores
B
GeoB19948-3
Melville Bugt
GeoB19927-3
Baffin Bay
Greenland
Disko Bugt
GeoB19905-1
Labrador Sea
Canada
Sea-ice extent:
September
August
October
July
November
June
December
May
April
January
February and March
Summer
Spring - Autumn
Winter
Cores (this study)
North Water Polynya

Fig. 1. A. Map of Baffin Bay and Labrador Sea areas with general surface circulation (warm surface current in red and cold polar sourced currents in blue) and locations of three sediment cores studied (GeoB19948-3, GeoB19927-3 and GeoB19905-1) herein, shown as red dots. B. The average maximum extent of the sea-ice edge for each month of the year (as per data from NSIDC 2012), adapted from Seidenkrantz (2013).

Bay-Labrador Sea region is a key location to study the interactions of sea ice, ice margin, and changes in sea-surface conditions (Fig. 1). Furthermore, it is of particular interest to investigate how climatic and oceanographic changes have affected sea-ice conditions along a north–south transect along the eastern Baffin Bay and Labrador Sea margin, from where long-term Holocene records are sparse (Briner *et al.* 2013; Gibb *et al.* 2015; Caron *et al.* 2019; Hansen *et al.* 2020; Saini *et al.* 2020).

In this study, we aim for a continuous Holocene climate record along a north–south transect through the eastern Baffin Bay-Labrador Sea from three sediment cores recovered from northern Baffin Bay (GeoB19948-3), NE Baffin Bay (GeoB19927-3; see also Saini *et al.* (2020)) and the NE Labrador Sea (GeoB19905-1), approximately representing the last 11.5 ka (Fig. 1). Special attention is given to high-resolution reconstructions of sea-ice conditions documented by the abundance and accumulation rates of IP_{25} and open-water phytoplankton biomarkers (brassicasterol, dinosterol and HBI III) as well as PIP_{25} indices. All data presented in this study are available at https://doi.pangaea.de/10.1594/PANGAEA.939206.

Environmental setting

The surface and subsurface waters in Baffin Bay and the Labrador Sea form a counter-clockwise gyre due to interaction of northward-flowing warm high salinity water transported by the West Greenland Current (WGC) with southward flowing cold polar sourced Arctic Water transported via the Baffin Current (BC) (Fig. 1A; Tang *et al.* 2004; Ribergaard *et al.* 2008). The WGC carries water from the warmer more saline western branch of the Irminger Current, modified by the less saline Arctic Water from the East Greenland Current (EGC) and local meltwater discharge along the SW Greenland coast. The WGC flows northwards along the west Greenland coast and typically turns west in the Melville Bugt before merging with the BC in northeastern Baffin Bay. The BC flows south along Baffin Island through Davis Strait before joining the Labrador Current (LC). In the western Labrador Sea, the LC overlies the WGC, which partly turns west and south again near Davis Strait.

Sea ice cover in Baffin Bay is variable and may range from 0 to ~10 months per year, with much of Baffin Bay covered by near-continuous sea ice during winter (Fig. 1B) (Tang *et al.* 2004). Ice growth first starts in northwestern Baffin Bay at the end of September and expands southeastwards, with a maximum extent in March, sometimes even reaching the NW Labrador Sea. After melting during the summer months it attains a minimal extent in September (Wang *et al.* 1994; Tang *et al.* 2004). The warm WGC negatively affects sea-ice formation and prevents its further growth along eastern Baffin Bay. A large interannual variability in sea ice has a major impact not only on ice conditions but on phytoplankton blooms and therefore marine productivity as well, which is coupled with the strong seasonality in surface air temperatures and wind patterns (Sakshaug 2004; Tang *et al.* 2004).

Material and methods

The three cores used in this study were collected during RV 'Maria S. Merian' cruise MSM44 (Dorschel *et al.* 2015). Site information, core lengths, and sampling intervals are provided in Table 1. Cores GeoB19948-3 and GeoB19927-3 were taken from northeastern Baffin Bay, whereas core GeoB19905-1 was taken from the northeastern Labrador Sea (Fig. 1, Table 1). Based on visual description and colour measurements of core GeoB19948-3 the upper 280 cm are mainly composed of olive-grey to silty clay homogeneous sediments (Dorschel *et al.* 2015). In core GeoB19927-3 the lowermost part is characterized by non-homogenous silt and fine sand sediments embedded with dropstones and sharp colour boundaries. The upper part of this core can be mainly described as homogenous olive-grey silty-clay sediments (Dorschel *et al.* 2015). In core GeoB19905-1, sediments are mainly composed of olive-grey muds with some sandy layers at the lower part of the core and sharp colour transitions displayed by distinct lithological units (LU); for a more detailed description, however, see Dorschel *et al.* (2015).

Table 1. Coordinates of the three cores used in this study.

Core ID	Region	Latitude (N)	Longitude (W)	Water depth (m)	Core length (cm)
GeoB19948-3	Northern Baffin Bay	75°46.10′	64°08.57′	778	1018
GeoB19927-3	Northeastern Baffin Bay	73°35.26′	58°05.66′	932	1147
GeoB19905-1	Eastern Labrador Sea	64°21.68′	52°57.70′	485	1045

Chronostratigraphy

The chronostratigraphical framework of the upper 280 cm of core GeoB19948-3 (Fig. 2) is based on four AMS ^{14}C dates measured on 0.57–1.12 mg of foraminifera from the >100 µm fraction (Table 2), performed directly on the CO_2 gas with the MICADAS (Mini Carbon Dating System) at the Alfred Wegener Institute in Bremerhaven, Germany (for methodological details see Wacker *et al.* 2013). Radionuclide analyses (^{210}Pb, ^{40}K, ^{137}Cs) were performed on core top sediments (depths 2, 6 and 10 cm) at the Bremen State Radioactivity Measurements Laboratory. Subsequently, the AMS dates were calibrated to calendar years using PaleoDataView (PDV) (Langner & Mulitza 2019), which uses modelled reservoir ages (Butzin *et al.* 2017; Table 1) to calibrate radiocarbon ages against IntCal13 (Reimer *et al.* 2013). The appropriate reservoir ages are chosen

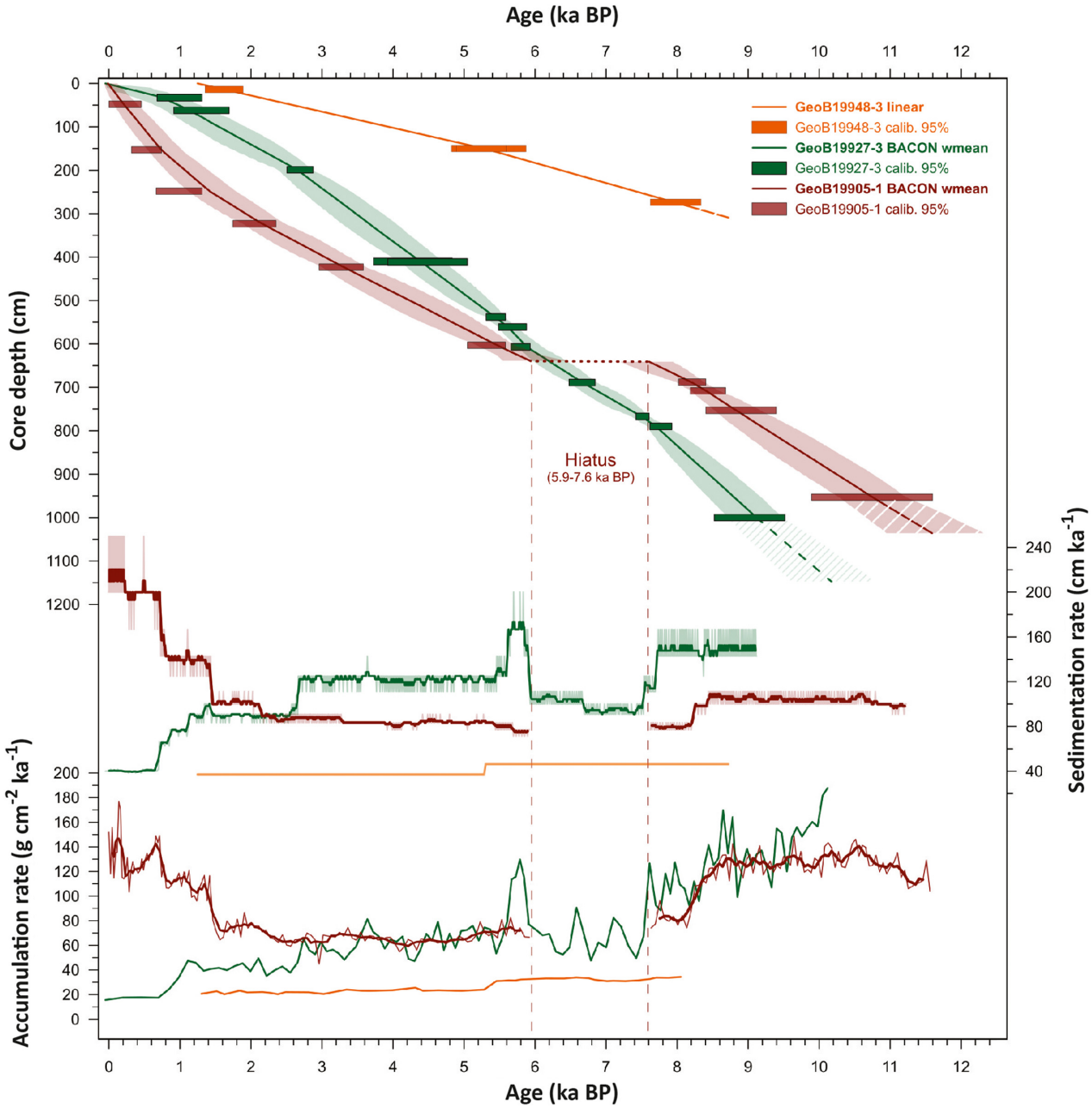

Fig. 2. Age models of GeoB19948-3 (orange), GeoB19927-3 (green) and GeoB19905-1 (red). For GeoB19927-3 and GeoB19905-1 the bold lines show weighted mean age after modelling in BACON, while the lighter shades indicate 95% confidence intervals (CIs). For GeoB19948-3 the age–depth relationship is given by linear interpolation between the AMS ^{14}C dates, shown as bold line. Stippled lines (GeoB19905-1) indicate areas of less robust age control. Rectangles denote 95% CIs of the AMS ^{14}C dates after calibration with PDV. In the centre and bottom panels the derived sedimentation and accumulation rates are shown, including 5-point running averages where applicable.

automatically based on the sample's radiocarbon age and location of the core. The calibrated ages were subsequently used to construct the final age model by linear interpolation between the calibrated ages and linear extrapolation between the topmost age and the core top. Due to the limited number of AMS ^{14}C dates, the age model is still preliminary.

The chronostratigraphy of core GeoB19927-3, previously published by Saini *et al.* (2020) (Fig. S1) is based on 12 AMS ^{14}C dates and radionuclide analyses (^{210}Pb, ^{40}K, ^{137}Cs) and was developed using 'BACON' software (Blaauw & Christen 2011) assuming a constant reservoir age of 140±35 years. However, to ensure consistency between the age models, we recalibrated the AMS dates (Fig. 2) using PDV (Butzin *et al.* 2017), which uses modelled reservoir ages to calibrate radiocarbon ages against IntCal13 (Reimer *et al.* 2013) (see Fig. S1 for comparison). According to the new age model, core GeoB19927-3 covers a time interval from *c.* 0 to 10.1 ka BP, which is almost the same as the original age model, i.e. only about 0.2 ka younger (Fig. S1).

The chronostratigraphy of core GeoB19905-1 (Fig. 2) is based on 12 AMS ^{14}C dates, previously published by Weiser *et al.* (2021) (see data sets available at https://doi.org/10.1016/j.quascirev.2021.106833). The age model was constructed using a combination of the PDV program (Langner & Mulitza 2019) and the open source software package BACON (Blaauw & Christen 2011). According to the published age model, core GeoB19905-1 covers a time interval from *c.* 0 to 11.5 ka BP, with a hiatus at depth 640 cm between 5.9 to 7.6 ka BP. For details on the methodological approach, the reader is referred to the original publication.

Bulk parameters (TOC and $CaCO_3$)

For organic-geochemical analyses, freeze-dried and homogenized subsamples were taken (n = 60, at 4-cm intervals for core GeoB19948-3 and n = 207, at 5-cm intervals for core GeoB19905-1) and stored in glass vials at −20 °C. TOC contents were measured using a carbon-sulphur ELTRA analyser (CS-800, ELTRA) after carbonate removal with hydrochloric acid (37%, 500 µL). The error of our TOC measurements is ±0.02%. The total amount of carbon (TC) was measured on untreated samples using a carbon-nitrogen-sulphur analyser (Elementar-III, Vario). Assuming the predominant carbonate phase is calcite, carbonate contents were calculated as $CaCO_3 = (TC - TOC) \times 8.333$, where 8.333 is the stoichiometric calculation factor.

Sea-ice biomarkers (IP_{25}, HBI III and sterols)

For biomarker analyses, we extracted ~4 g of freeze-dried and homogenized sediment using dichloromethane: methanol (2:1 v/v) as a solvent for ultrasonication (3×15 min). Prior to extraction, 9-octylheptadec-8-ene (9-OHD; 0.1 µg per sample), 7-hexylnonadecane (7-HND; 0.076 µg per sample), 5α-androstan-3β-ol (androstanol; 10.7 µg per sample) and 2,6,10,15,19,23-hexamethyltetracosane (squalane; 3.2 µg per sample) were added for quantification of biomarkers. The extracts were separated by open silica (SiO_2) column chromatography with *n*-hexane (5 mL) and ethylacetate: *n*-hexane (9 ml, 2:8 v/v) as eluent into the hydrocarbon and sterol fractions, respectively. The sterol fraction was silylated using 200 µl bis-trimethylsilyltrifluoroacet-amide (BSTFA; 60 °C, 2 h).

Two different gas chromatography-mass spectrometers (GC-MS) with similar basic configuration were used to qualify and quantify the hydrocarbon and sterol fractions. The quantification of the HBI fraction was carried out with a gas chromatograph (Agilent Technologies GC6850, 30 m DB-1MS column, 0.25 mm id, 0.25 µm film) coupled to an Agilent Technologies 5977C VL MSD mass selective detector (Triple-Axis Detector, 70 eV constant ionization potential, scan 50–550 m z^{-1}, 1 scan s^{-1}, ion source temperature 230 °C). The quantification of the sterols (quantified as trimethylsilyl ethers) was carried out with a GC Agilent 6850 (30 m DB-1MS column, 0.25 mm id, 0.25 µm film) coupled to an Agilent 5975C VL MSD mass selective detector. GC measurements were carried out with the following temperature programme: 60 °C (3 min), 150 °C (15 °C min^{-1}), 320 °C (10 °C min^{-1}), 320 °C (15 min isothermal) for the hydrocarbons and 60 °C (2 min), 150 °C (15 °C min^{-1}), 320 °C (3 °C min^{-1}), 320 °C (20 min isothermal) for the sterols. Helium served as

Table 2. Results of the AMS dating and subsequent calibration from core GeoB19948-3. Reservoir ages are in respect to IntCal13, min. and max. ages respectively correspond to the 5% and 95% confidence intervals defined by PDV. The last column denotes the final ages used for the stratigraphical framework.

AMS dating, MICADAS, AWI Bremerhaven					Reservoir correction and calibration, PaleoDataView			
Lab. ID AWI-	Depth (cm)	^{14}C age (a BP)	^{14}C error (a)	Material	Reservoir age (a)	Min. age (cal. a BP)	Max. age (cal. a BP)	Weighted mean age (cal. a BP)
1252.1.1	14	2443	108	Mixed foraminifera	734±64	1354	1890	1625
1253.2.1	150	5431	198	Mixed benthic foraminifera	818±58	4824	5874	5281
1253.1.1	150	5427	114	*N. pachyderma* sin	818±58	4892	5591	5285
1475.1.1	274	7789	184	Mixed foraminifera	660±61	7623	8336	7965

carrier gas (1 mL min^{-1} constant flow). Specific compound identification was based on the comparison of gas chromatography retention times with those of reference compounds and published mass spectra (Boon *et al.* 1979; Volkman 1986; Belt *et al.* 2007; Brown & Belt 2016). For the quantification of IP_{25} and HBI III (Z-isomer, generally referred to as 'HBI III') their molecular ion ratio (m z^{-1} 350 for IP_{25} and m z^{-1} 346 for HBI III in relation to the abundant fragment ion m z^{-1} 266 of internal standard (7-HND)) was used (in selected ion monitoring mode, SIM). The different responses of these ions and a detailed quantification method are given by Fahl & Stein (2012). For the quantification of the sterols, the molecular ions m z^{-1} 470 for brassicasterol (as 24-methylcholesta-5,22E-dien-3β-o-Si$(CH_3)_3$) and m z^{-1} 500 for dinosterol (4α,23,24R-trimethyl-5α-cholest-22E-en-3β-o-Si$(CH_3)_3$) were used in relation to the molecular ion m z^{-1} 348 for the internal standard androstanol.

The PIP_{25} indices were calculated by combining IP_{25} with different phytoplankton markers for semi-quantitative sea-ice reconstruction according to Müller *et al.* (2011):

$$PIP_{25} = \frac{[IP_{25}]}{([IP_{25} + c \times p])} \quad (1)$$

where c = mean $[IP_{25}]$/mean $[p]$ and p is the phytoplankton biomarker content (p = B (brassicasterol) or D (dinosterol) or III (HBI III)). Recently, based on surface sediments from Baffin Bay, Kolling *et al.* (2020) suggested that sea-ice indices P_DIP_{25} and P_BIP_{25} may indicate late spring and/or autumn conditions, while $P_{III}IP_{25}$ may record more the early spring and/or late winter (ice-edge) conditions. Here we concentrate on the $P_{III}IP_{25}$ as for this proxy other published records from Baffin Bay are also available. For P_DIP_{25} and P_BIP_{25} see Saini *et al.* (2020) and the complete data at https://doi.pangaea.de/10.1594/PANGAEA.911365.

Calculation of accumulation rates

Biomarker contents were converted into accumulation rates by using the following equations (e.g. Stein & Macdonald 2004):

$$Bulk\ AR = LSR \times DBD \quad (2)$$

$$TOC\ AR = Bulk\ AR \times TOC/100 \quad (3)$$

$$CaCO_3\ AR = Bulk\ AR \times CaCO_3/100 \quad (4)$$

$$BMAR = Bulk\ AR \times BM \quad (5)$$

where LSR = sedimentation rate (cm ka^{-1}), DBD = dry bulk density (g cm^{-3}), TOC = total organic carbon content (%), $CaCO_3$ = carbonate content (%), BM = biomarker content (μg g^{-1}), bulk AR = total sediments accumulation rate (g cm^{-2} ka^{-1}), TOC AR = total organic carbon accumulation rate (g cm^{-2} ka^{-1}), $CaCO_3$ AR = carbonate accumulation rate (g cm^{-2} ka^{-1}), and BMAR = biomarker accumulation rate (μg cm^{-2} ka^{-1}).

Results

Core chronology and sedimentation rates

Core GeoB19948-3. – Given the scarcity of calcareous material in the sediment resulting in only four AMS ^{14}C dates for core GeoB19948-3, only a preliminary chronological framework could be constructed. Still, this framework suggests continuous sedimentation since ~8 ka BP (Fig. 2), with sedimentation rates in the order of 40–50 cm ka^{-1}. No excess ^{210}Pb and/or ^{137}Cs were found in the top sediments and thus the age of the topmost date (1.6 ka BP, 14 cm core depth) suggests that the core top is not of recent age, but instead ~1.2 ka old.

Core GeoB19927-3. – The updated age model of core GeoB19927-3 suggests continuous sedimentation since ~10.1 ka BP (Fig. 2). Sedimentation rates vary between 40 and 200 cm ka^{-1}, although high sedimentation rates of about 100–200 cm ka^{-1} prevail in the majority of the record, except for a prominent decrease starting at 2.6 ka BP leading to low values of <50 cm ka^{-1} after 0.7 ka to present.

Core GeoB19905-1. – The age model of core GeoB19905-1 (Weiser *et al.* 2021) suggests continuous sedimentation from 11.5 to 7.6 ka BP and since 5.9 ka BP (Fig. 2). A hiatus spanning about 1.7 ka in between these intervals was identified at 640 cm core depth. Sedimentation rates range from 71 to 250 cm ka^{-1} with high values of ~100 cm ka^{-1} between 11.5–8.2 ka BP and decreasing to about 80 cm ka^{-1} from 8.2–7.6 and 5.9–2.4 ka BP. A strong increase in sedimentation rates to 80–100 cm ka^{-1} is recorded after 2.4 ka BP that rises even further up to 150, 200 and 250 cm ka^{-1} after 1.4, 0.7 and 0.3 ka BP, respectively.

Organic geochemical bulk parameters and biomarkers

The organic-geochemical and biomarker records of core GeoB19927-3, excluding $CaCO_3$, have already been described and published by Saini *et al.* (2020). Thus, here only the new data of cores GeoB19948-3 and GeoB19905-1 are presented. In the discussion, however, data from all three cores are included. The results of all biomarkers contents are plotted in μg g^{-1} TOC and as accumulation rates in μg cm^{-2} ka^{-1} (Figs S3, S4). They are also presented in μg g^{-1} sediment in Figs S2–S4. The distribution of contents and accumulation rates of

biomarkers and bulk parameters reveal significant down-core variations.

Core GeoB19948-3. – The GeoB19948-3 record presented here extends to ~8 ka BP. $CaCO_3$ contents vary between 3.6 to 1% over the last ~8 ka (Fig. 3B). Higher values of about 2.4% (mean) occur from *c.* 8 to 5.3 ka BP followed by lower contents of 1.9% (mean) towards the top of the core. TOC contents vary between about 0.8 to 0.4% over the last ~8 ka (Fig. 3D), and display higher values of about 0.7% (mean) from *c.* 8 to 5.3 ka BP, followed by lower contents of 0.6% (mean) towards the top of the core. HBI III contents were typically near zero over the last ~8 ka, except for two prominent peaks of 0.6 and 0.4 μg g^{-1} TOC at about 6.5 and 1.6 ka BP, respectively (Fig. 3F). The phytoplankton sterols dinosterol and brassicasterol display higher contents from 8 to 5.3 ka BP, followed by a gradual decrease towards the top of the core (Fig. 3H, J). IP_{25} contents vary between 0.2 and 2.0 μg g^{-1} TOC and display higher values from 8 to 5.3 ka BP, followed by lower values towards the core top (Fig. 3L).

The accumulation rates of TOC range from 0.10 to 0.26 g cm^{-2} ka^{-1} and are marked by a gradual decrease from *c.* 8 to 1.2 ka BP (Fig. 3E). The $CaCO_3$ accumulation rates show a similar generally decreasing trend from 8 to 1.2 ka BP and vary between about 0.2 to 1 g cm^{-2} ka^{-1} (Fig. 3C). HBI III accumulation rates are typically low (near zero) throughout the Middle-to-Late Holocene (mean ~0.02 μg cm^{-2} ka^{-1}; Fig. 3G), except for a prominent peak around 6.7–6.3 ka BP. This peak value, however, should be interpreted with caution due to the limited number of AMS ^{14}C dates. The accumulation rates of the phytoplankton biomarkers dinosterol and brassicasterol vary between 0.7 and 5.7 μg cm^{-2} ka^{-1} and show a gradual decrease from *c.* 8–1.2 ka BP (Fig. 3I, K). IP_{25} accumulations rates range between 0.03 and 0.5 μg cm^{-2} ka^{-1} and are relatively high in the early part of the Middle Holocene between 8–5.3 ka BP, followed by constantly low values between *c.* 5.3–1.2 ka

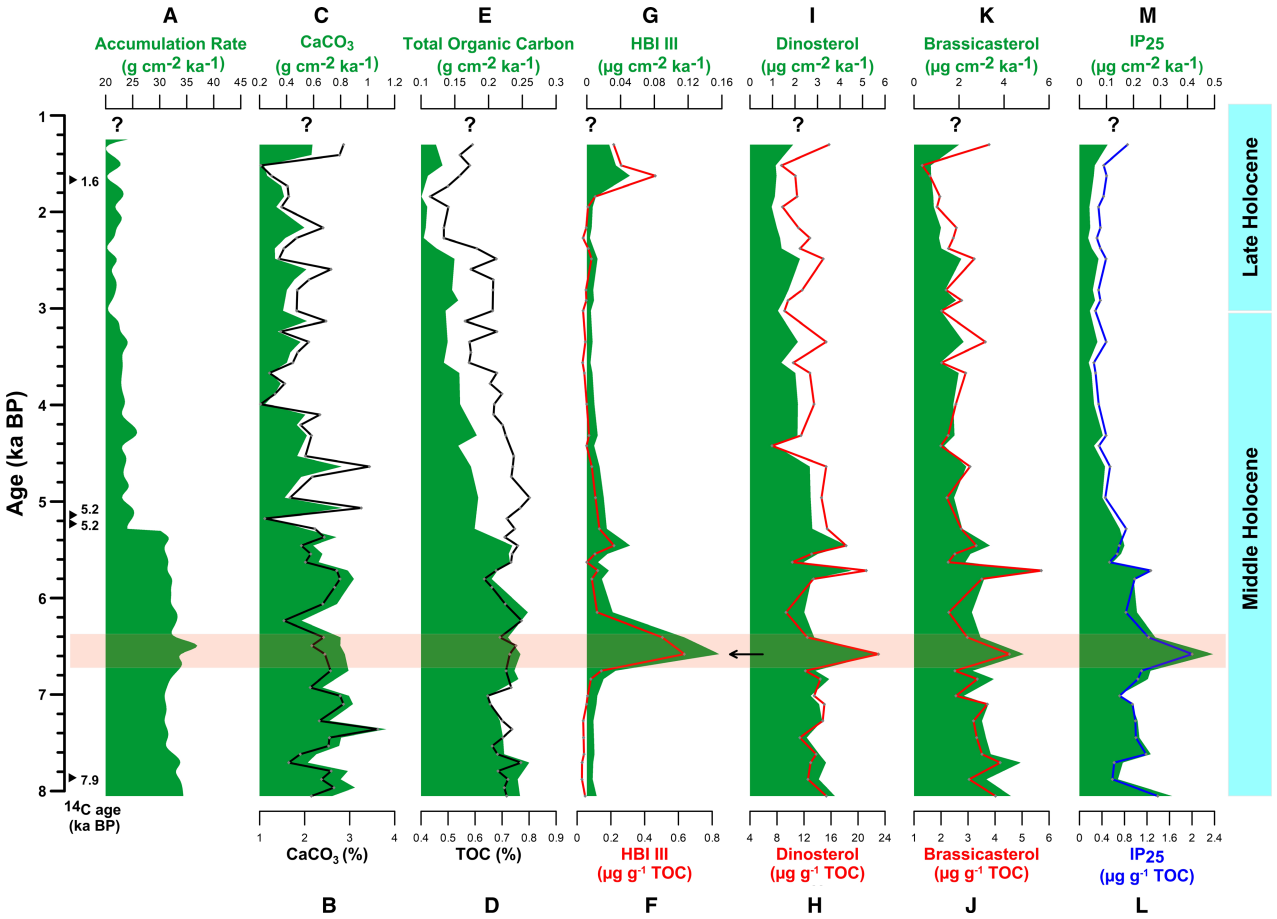

Fig. 3. Records of core GeoB19948-3 including bulk parameters and biomarkers and their accumulation rates. A. Bulk accumulation rate. B. $CaCO_3$ content. C. $CaCO_3$ accumulation rate. D. Total organic carbon (TOC) content. E. TOC accumulation rate. F. HBI III (μg g^{-1} TOC). G. HBI III accumulation rate. H. Dinosterol (μg g^{-1} TOC). I. Dinosterol accumulation rate. J. Brassicasterol (μg g^{-1} TOC). K. Brassicasterol accumulation rate. L. IP_{25} (μg g^{-1} TOC). M. IP_{25} accumulation rate. Black solid triangles mark the AMS ^{14}C dates. All plots are shown vs. age in 1000 years before present (ka BP).

BP (Fig. 3M). The $P_{III}IP_{25}$ index varies in the range 0.1 to 0.8 and displays higher values in the Early Holocene prior to 7.6 ka BP; show decreased values in the Middle Holocene from *c.* 7.6 to 3 ka BP, followed by generally reduced values in the Late Holocene (Fig. 5H). Moreover, $P_{III}IP_{25}$ attains two minimum values of ~0.29 and ~0.15 at about 6.7–6.3 (Middle Holocene) and ~1.8–1.3 ka BP (Late Holocene), respectively.

Core GeoB19905-1. – TOC contents vary between 0.2 and 2.4%, showing the lowest values between ~11.5 to 8.2 ka BP followed by a sharp rise afterwards, and acquire their highest (mean 1.8%) values during the last *c.* 5 ka (Fig. 4B). $CaCO_3$ contents range from 0.7 to 21.8% throughout the record and display continuously low values of about 3.3% (mean) between ~11.5 and 9.1 ka BP (Fig. 4D). They increase to maximum values of 21%, attaining the maximum at about 4.4 ka BP and drop to generally lower values (mean 3.3%) between 2.1 to 0.4 ka BP, followed by a minor rise to about 5% (mean) in the upper part of the core in the last *c.* 0.4 ka BP. The phytoplankton biomarkers dinosterol and brassicasterol co-vary between 3 and 43 μg g^{-1} TOC throughout the Holocene (Fig. 4F, H). Phases with variable but high values (mean 11.4 μg g^{-1} TOC) of dinosterol and brassicasterol were observed between ~11.5 and 8.6 ka BP; however, they show no increase in μg g^{-1} sediment in this period (Fig. S4). A slight decrease in dinosterol contents

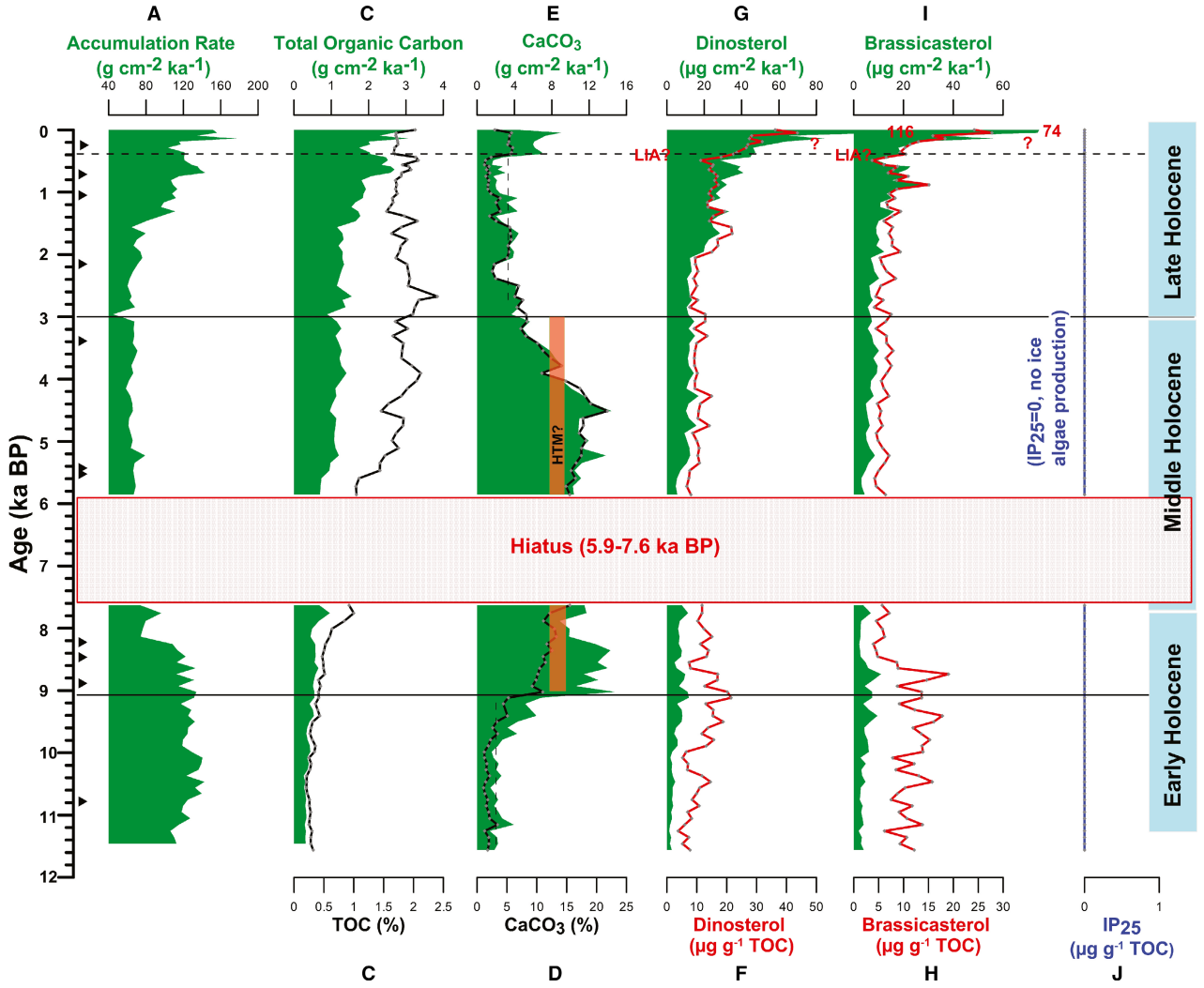

Fig. 4. Records of core GeoB19905-1 including bulk parameters and biomarkers and their accumulation rates. A. Bulk accumulation rate. B. Total organic carbon (TOC) content. C. TOC accumulation rate. D. $CaCO_3$ content. E. $CaCO_3$ accumulation rate. F. Dinosterol (μg g^{-1} TOC). G. Dinosterol accumulation rate. H. Brassicasterol (μg g^{-1} TOC). I. Brassicasterol accumulation rate. J. IP_{25} (μg g^{-1} TOC). The orange bar indicates the maximum occurrence of mixed planktic and benthic foraminifera specimens in this core (J. Weiser, pers. comm. 2021). High accumulation rates at the top (last *c.* 0.4 ka) may indicate enhanced primary production and/or preservation but the possibility of diagenetic alteration in the upper ~100 cm cannot be excluded (cf. Discussion for further explanation). Black solid triangles mark the AMS ^{14}C dates. All plots are shown vs. age in 1000 years before present (ka BP).

(mean 10.4 μg g^{-1} TOC) occurs between 8.6–7.6 and 5.9–2.1 ka BP. Afterwards, a strong increase in dinosterol content is recorded from 2.1–0.4 ka BP followed by an even stronger rise to about 40 μg g^{-1} TOC during the last *c*. 0.4 ka BP. IP_{25} and HBI III are absent throughout the record of the last 11.5 ka BP (Fig. 4J).

The accumulation rates of TOC, $CaCO_3$ and phytoplankton biomarkers dinosterol and brassicasterol vary between about 0.2–3 g cm^{-2} ka^{-1}, 1–14 g cm^{-2} ka^{-1}, 1–116 μg cm^{-2} ka^{-1} and 2–74 μg cm^{-2} ka^{-1}, respectively (Fig. 4C, E, G, I). IP_{25} accumulation rates are zero (as $IP_{25} = 0$) throughout the record (Fig. 4J). Overall, the accumulation rates of TOC and the phytoplankton biomarkers dinosterol and brassicasterol remain relatively low and constant until about 7.6 ka BP and show slightly increased values from 5.9 to about 2 ka BP. A period of a strong increase in the accumulation rates of dinosterol and brassicasterol followed during the last ~2 ka BP. However, TOC accumulation rates remain relatively low until about 1.5 ka BP and show a strong increase during the last 1.5 ka BP. During the last *c*. 0.4 ka BP, the highest accumulation rates of TOC, dinosterol and brassicasterol were recorded. $CaCO_3$ accumulation rates are low until 9.1 ka BP, followed by increased and maximum values from 9.1–7.6 and 5.9–3.0 ka BP and thereafter decrease during the last 3 ka, except for a minor rise during the last 0.4 ka BP.

Discussion

In order to investigate the palaeoceanographic changes along a N–S transect through eastern Baffin Bay to the Labrador Sea margin on the West Greenland Shelf, we have used a combination of sea ice, open-water phytoplankton productivity biomarkers and organic geochemical bulk parameters that are discussed together with relevant literature data. The records from this study show variability in sea-ice conditions along this north–south transect (Figs 5, 6) throughout the Holocene.

Deglacial to Early Holocene (11.5–7.6 ka BP)

Minimum occurrence or even absence of ice algae and phytoplankton biomarkers (cf. Saini *et al*. 2020) and related high $P_{III}IP_{25}$ indices (Fig. 5G) in core GeoB19927-3 in Baffin Bay suggest (early) spring conditions with extensive (spring) SIC prior to 7.6 ka BP. Primary productivity indicators in cores GeoB19927-3; AMD14-204C (Fig. 7E, F) show relatively low values in this period, suggesting a low productive environment (Limoges *et al*. 2020). Previous studies based on marine sediment cores from Baffin Bay have suggested that this region was controlled by cold deglacial conditions prior to *c*. 7.6 ka BP, especially during the initial part of the Early Holocene (Caron *et al*. 2019; Georgiadis *et al*. 2020; Hansen *et al*. 2020; Limoges *et al*. 2020). High $P_{III}IP_{25}$ index values (~0.9) prior to 7.6 ka BP from a nearby core AMD14-204C (Limoges *et al*. 2020) located in eastern Baffin Bay also suggest extended (early) spring sea-ice conditions (Fig. 5E). These generally harsh conditions were further supported by high IRD counts and extensive SIC (>10 months per year) as per reconstructions from eastern Baffin Bay (core CC70) in this period (Jennings *et al*. 2014; Gibb *et al*. 2015; Fig. 10A). Furthermore, extended sea-ice conditions (with generally reduced primary production; Fig. 7E, F) between ~8.8–7.6 ka BP in Baffin Bay (core GeoB19927-3; Saini *et al*. 2020) were reported and may be associated with the opening of Nares Strait and the inflow of cold Polar Water into Baffin Bay (Jennings 1993; Georgiadis *et al*. 2018; Jennings *et al*. 2019; Saini *et al*. 2020).

However, prior to ~9.1 ka BP, the surface and subsurface conditions in the NE Labrador Sea (core GeoB19905-1) are characterized by the absence of ice algae biomarkers as well as by extremely low accumulation rates of $CaCO_3$ and phytoplankton biomarkers (Fig. 8D, F, G). These (spring, summer and autumn) ice-free, albeit low primary productivity conditions might be related to the limited presence of warm Atlantic Water in the surface waters together with relatively high deglacial meltwater discharge (Fig. 8C, H; Weiser *et al*. 2021) from the adjacent ice sheets. Such conditions might be attributed to the rapid retreat of the Greenland Ice Sheet (GIS) from the West Greenland Shelf (Andrews *et al*. 1999; Briner *et al*. 2016; Fig. 10A). Based on dinocyst reconstructions in the vicinity (core SA13-ST3), Allan *et al*. (2021) have reported generally low sea ice cover (<6 months per year) in the last 11 ka BP (Fig. 5B), possibly in winter months only. The occurrence of the dinocyst *Pentapharsodinium dalei* in core CC70 off Disko Bugt indicates large seasonal gradients from cold winters to mild summers and is possibly related to salinity fluctuations induced by meltwater discharge from the retreating GIS. This might indicate a weaker influence of the Atlantic Water (WGC) in the central Baffin Bay region (Gibb *et al*. 2015), in agreement with our reconstructions in the Labrador Sea (Figs 7, 8).

In the interval after ~9.1 ka BP, the NE Labrador Sea (core GeoB19905-1) is marked by an increase in the accumulation rates of $CaCO_3$ and the phytoplankton biomarker dinosterol as well as the absence of ice algae biomarkers (Fig. 4), all pointing towards increased marine productivity and ice-free conditions, which might correlate with the onset of the Holocene Thermal Maximum (HTM) conditions (Kaufman *et al*. 2004). Maximum occurrence of mixed benthic and planktic foraminifera specimens from the same core (GeoB19905-1) in this interval also points towards increased surface to subsurface productivity (Fig. 8). This might be also related to the disappearance of multi-year sea ice, which may have released an additional input of sympagic carbon into the water column further

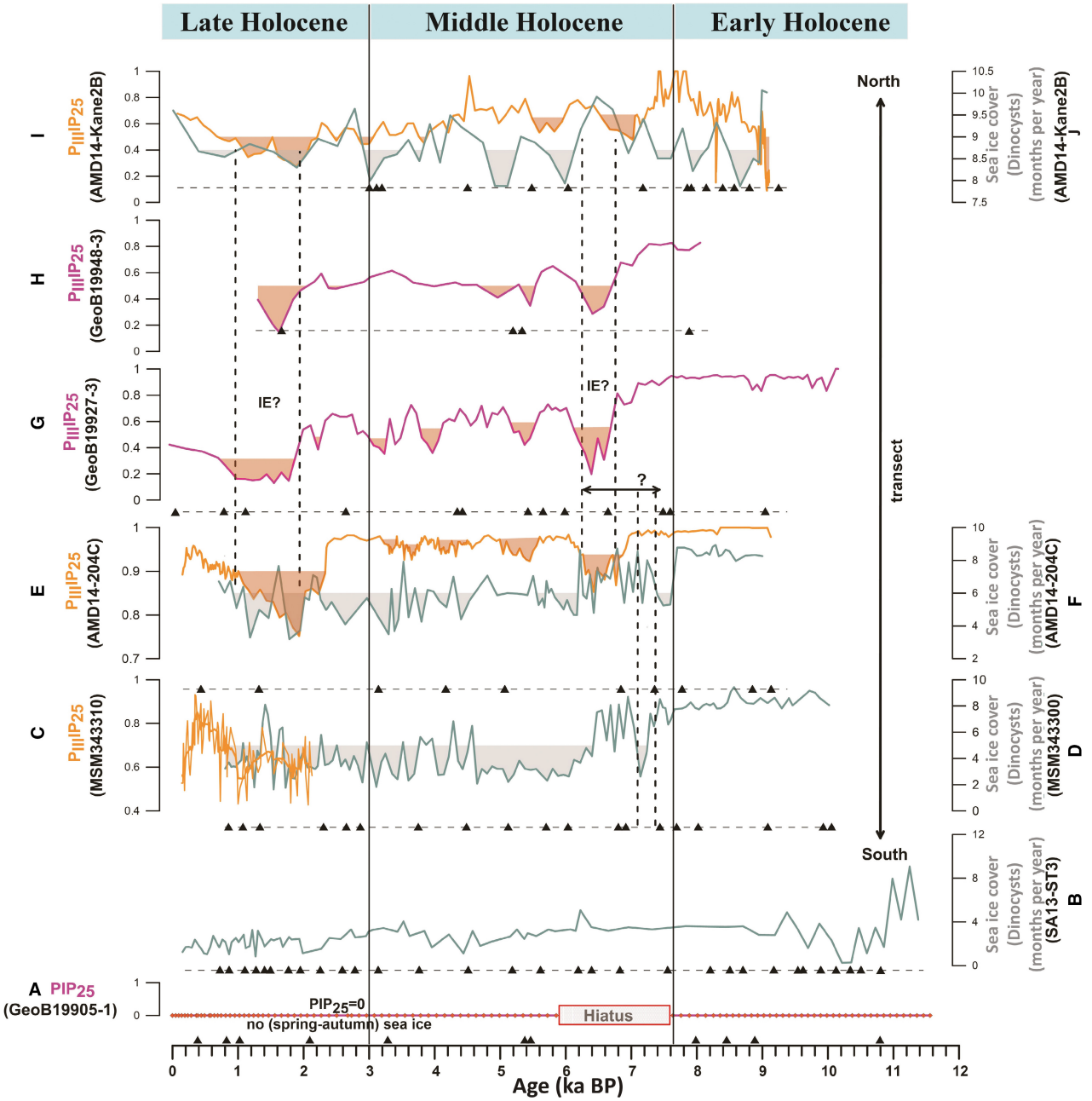

Fig. 5. Comparison of different sea-ice records based on $P_{III}IP_{25}$ and dinocyst records along the eastern Baffin Bay–Labrador Sea (N–S) transect. A. Core GeoB19905-1 (this study). B. Core SA13-ST3 (Allan *et al.* 2021). C. Core MSM343310 (Kolling *et al.* 2018). D. Core MSM343300 (Ouellet-Bernier *et al.* 2014). E, F. Core AMD14-204C (Caron *et al.* 2019; Limoges *et al.* 2020). G. Core GeoB19927-3 (Saini *et al.* 2020). H. GeoB19948-3 (this study). I, J. Core AMD14-Kane2B (Caron *et al.* 2019; Georgiadis *et al.* 2020). Orange shading in PIP_{25} records might be interpreted as ice-edge (IE?) situations (cf. Saini *et al.* 2020). The positions of these cores are indicated in Fig. 1. Calibrated AMS ^{14}C ages of cores with varying age-resolution are shown as solid triangles for correct correlation of data.

driving high marine productivity (Yunda-Guarin *et al.* 2020). This increase in primary productivity was most likely associated with a strong inflow of Atlantic Water and a decreased meltwater input (Fig. 8C, H; Weiser *et al.* 2021) and therefore, strengthened WGC influence from ~9.1 ka BP onwards (Fig. 10B) penetrating up to northern Baffin Bay (Lloyd *et al.* 2005; Saini *et al.* 2020). Based on an increase in salinity and reduction in SIC from the outer shelf of Disko Bugt (core CC70), Jennings *et al.* (2014) and Gibb *et al.* (2015) suggested diminution of GIS meltwater input into the West Greenland areas. This rapid retreat of the GIS ice margin, thinning of ice sheets and spring–autumn ice-free conditions related to the strong oceanic forcing and high summer insolation in

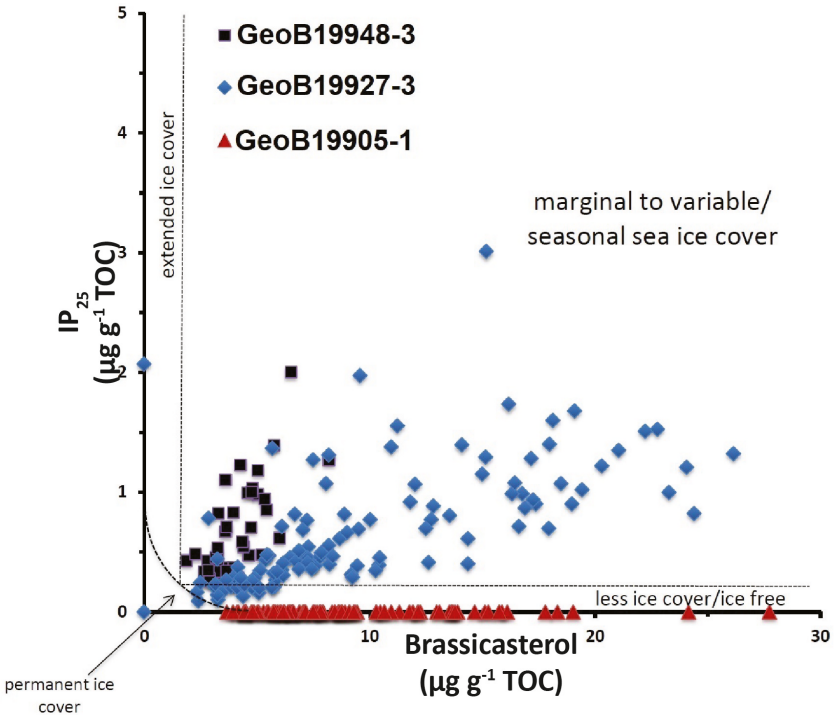

Fig. 6. Correlation of IP_{25} vs. phytoplankton brassicasterol based on GeoB19948-3, GeoB19927-3 and GeoB19905-1, indicating variable seasonal to marginal ice-edge to ice-free conditions along the eastern Baffin Bay–Labrador Sea (north–south) transect. See Müller *et al.* (2011) for the classification of different sea-ice scenarios (cf. Discussion for further explanation).

the Early Holocene correspond well to the significant climate warming (Lloyd *et al.* 2005; Vinther *et al.* 2009; Renssen *et al.* 2012), widely recognized in the North Atlantic and western Arctic (Kaufman *et al.* 2004). Syring *et al.* (2020) and Müller & Stein (2014) also implied reduced SIC conditions (Fig. 9), as a result of strong inflow of warmer Atlantic Water in the Fram Strait area (Werner *et al.* 2016), in agreement with our reconstructions from the eastern margin of the Labrador Sea and Baffin Bay.

Middle Holocene – transition to full interglacial conditions (7.6–3.0 ka BP)

During the Middle Holocene ~7.6 ka BP, SIC started to decrease in Baffin Bay as shown by reduced values of $P_{III}IP_{25}$ indices in cores GeoB19927-3 and GeoB19948-3 (Fig. 7D). This reduction in SIC was likely accompanied by strongly reduced meltwater input, causing increased surface salinity (Fig. 9), despite a decrease in subsurface Atlantic Water inflow (Fig. 8H; Weiser *et al.* 2021). In sum, this can be explained by assuming an increased influence of Atlantic Water on the surface water (Fig. 10B). This resulted in increased primary productivity as displayed by high peaks in productivity indicators (Fig. 8F, G). Short-term (cyclic) changes of minima and maxima in SIC are evident after ~7.6 ka BP in Baffin Bay, displayed by the $P_{III}IP_{25}$ index (Fig. 5) based on Baffin Bay sediment cores GeoB19927-3 and GeoB19948-3. These reoccurring spring ice-edge conditions based on simultaneous peaks in accumulation rates of IP_{25} and the phytoplankton biomarkers brassicasterol and dinosterol (Fig. S2) are possibly related to oscillations in the ice melt influx and the influence of the WGC in the surface waters (Caron *et al.* 2019; Hansen *et al.* 2020). Additionally, the $P_{III}IP_{25}$ index values along this north–south transect in eastern Baffin Bay (core GeoB19927-3, GeoB19948-3, AMD14-Kane2B; Fig. 5) indicate a prominent decline in SIC starting from ~7.6–6.3 ka BP. Based on dinoflagellate cyst data from core CC70, Gibb *et al.* (2015) reported an increased winter SST at ~7.6 ka BP associated with the strengthening of the warmer Atlantic Water influence that might further support our reconstruction. However, increased HBI III fluxes in nearby cores AMD14-Kane2B and AMD14-204C during this interval might be indicative of increased mobile sea ice and freshwater outflow via Nares Strait (Georgiadis *et al.* 2020; Limoges *et al.* 2020). Interestingly, dinocysts based sea-ice reconstructions from Disko Bugt (core MSM343310) in eastern Baffin Bay exhibit a similar reduction in SIC from 7.5–7.1 ka BP (cores GeoB19927-3, GeoB19948-3, AMD14-Kane2B). However, different reservoir ages (a few hundred to sometimes a thousand years) may limit the

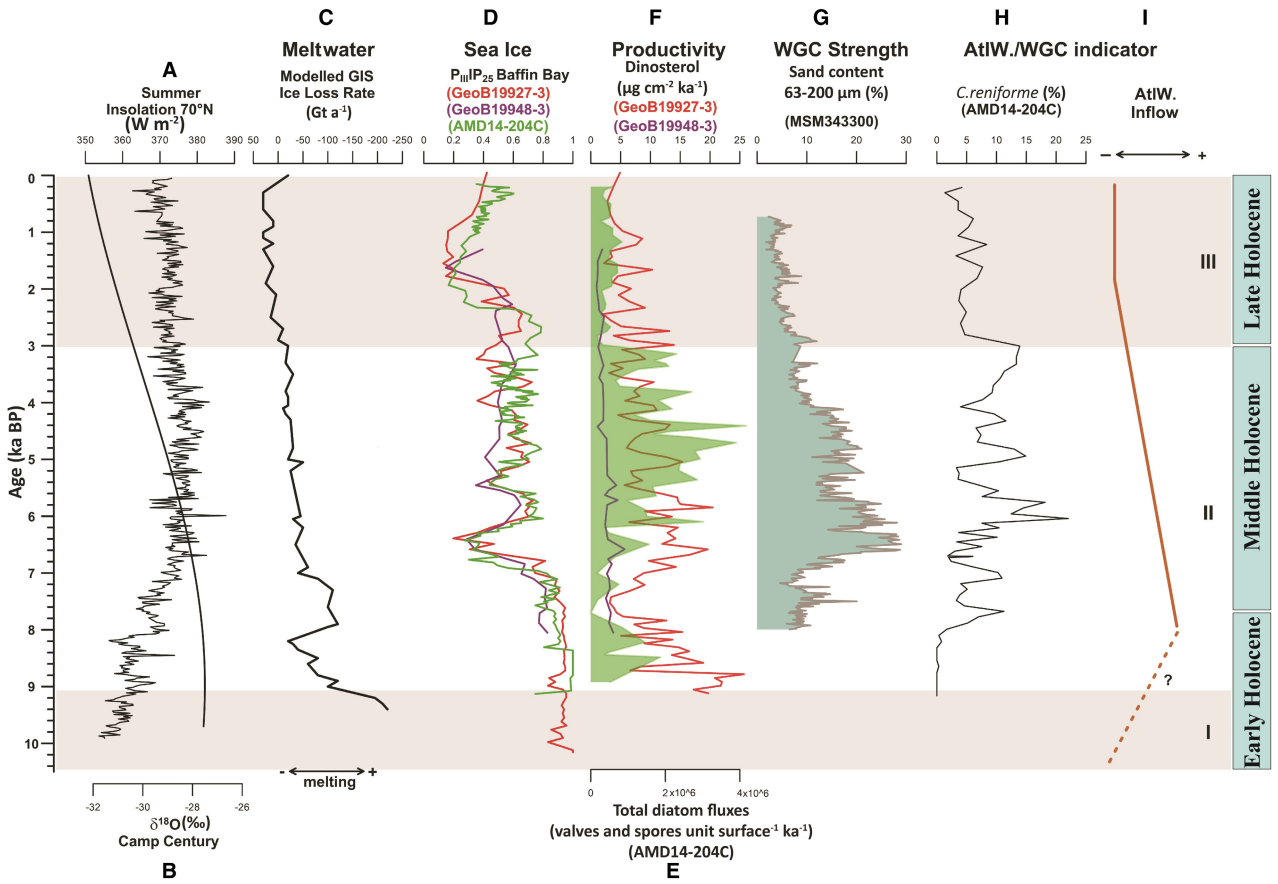

Fig. 7. Comparison of selected proxies for sea ice from Baffin Bay with proxies for the productivity, inflow of warm Atlantic Water (AtlW.)/WGC strengths and meltwater from circum Baffin Bay area's. A. Summer insolation at 70°N (Laskar *et al.* 2004). B. Camp Century $\delta^{18}O$ record (Vinther *et al.* 2009). C. Modelled GIS ice loss rate (Lecavalier *et al.* 2014). D. Sea-ice indicator; $P_{III}IP_{25}$ from cores GeoB19927-3 (Saini *et al.* 2020), GeoB19948-3 and AMD14-204C (Limoges *et al.* 2020). E. Total diatom fluxes; core AMD14-204C (Limoges *et al.* 2020). F. Dinosterol accumulation rate; cores GeoB19927-3 (Saini *et al.* 2020) and GeoB19948-3. G. Core MSM343300 (Perner *et al.* 2012). H. Core AMD14-204C (Hansen *et al.* 2020). I. Qualitative reconstruction of AtlW. inflow into northeastern Baffin Bay. I to III represent different environmental periods shown in the maps of Fig. 10, based on our proxy records.

exact age correlation (Fig. 5; Caron *et al.* 2019; Georgiadis *et al.* 2020; Hansen *et al.* 2020; Saini *et al.* 2020). On the other hand, the reduced SIC may have occurred earlier in the southern areas of the Baffin Bay transect (7.5–7.1 ka BP) before penetrating northwards up to the Kane Basin. Based on diatom and biomarker data from core AMD14-204C, Limoges *et al.* (2020) also suggested decreased sea-ice conditions with increased primary production, possibly due to increased WGC influence during this interval. The decreased SIC (Fig. 7D) after ~7.6 ka BP, together with high Atlantic Water influence associated with a decreased inflow of meltwater, might suggest significant warming of the subsurface conditions corresponding to the HTM-like conditions observed in NE Baffin Bay throughout the Middle Holocene (Lloyd *et al.* 2005; Gibb *et al.* 2015; Fig. 10B). Several records from circum Greenland, the Canadian Arctic Archipelago, and Svalbard areas also suggested a similar increased influence of Atlantic Water (WGC, IC) in the Middle Holocene since ~7.6 ka BP (Dyke *et al.* 1996; Justwan *et al.* 2008; Jennings *et al.* 2011; Ouellet-Bernier *et al.* 2014). Note, in contrast to sea-ice records from the Fram Strait area (cores MSM5/5-712 and PS93/025), which seem to follow predominantly the summer insolation trend (Müller *et al.* 2012; Syring *et al.* 2020), our records from eastern Baffin Bay indicate a dominant influence of meltwater influx on sea-ice formation throughout the Holocene (Fig. 9).

Furthermore, a general northwards increase in SIC shown by the PIP_{25} indices along the studied N–S transect (Figs 5, 6) might be related to the fading Atlantic Water inflow (WGC) northwards and/or due to interaction with southwards flowing Polar Currents (PC) along the Baffin Islands (Canadian Arctic). This trend may also be related to the seasonal differences in light and sea-ice conditions as a function of latitude as the timing and extent of the ice and phytoplankton productivity vary from April to late summer from the south towards higher latitudes (cf. Wassmann *et al.* 2020 for a detailed explanation).

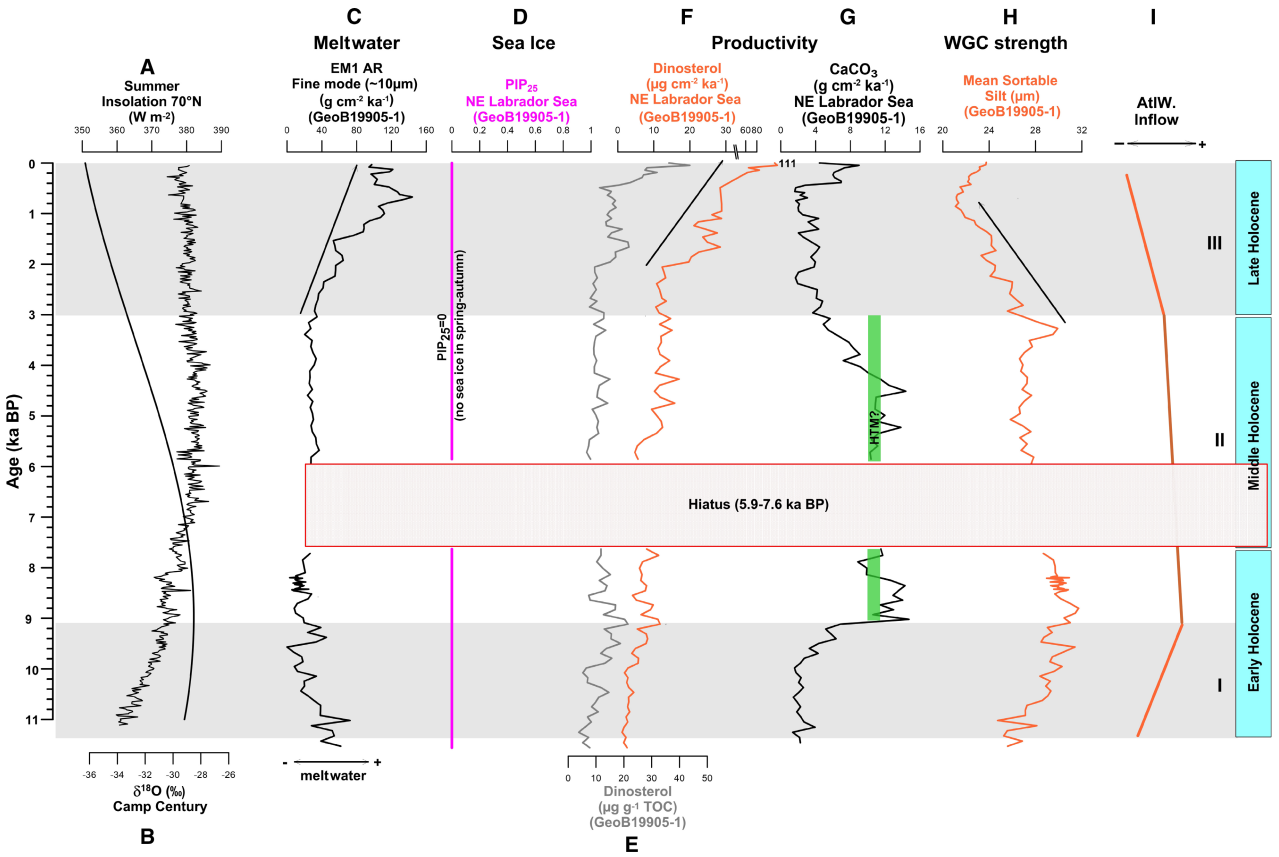

Fig. 8. Comparison of selected proxies for sea ice with productivity, WGC current strengths in the NE Labrador Sea and/or inflow of warm Atlantic Water (AtlW.) as well as meltwater influence in the area. A. Summer insolation at 70°N (Laskar *et al.* 2004). B. Camp Century $\delta^{18}O$ record (Vinther *et al.* 2009). C. Core GeoB19905-1 fine grain size mode AR (EM1) accumulation rate (Weiser *et al.* 2021). D. Core GeoB19905-1 sea ice ($PIP_{25} = 0$). E. Core GeoB19905-1 dinosterol (µg g^{-1} TOC). F, G. Core GeoB19905-1 productivity (dinosterol and $CaCO_3$; accumulation rates). H. Core GeoB19905-1, $\overline{SS}$ (mean sortable silt) (Weiser *et al.* 2021). I. Qualitative assessment of the AtlW. inflow into the NE Labrador Sea. The green bar indicates the maximum occurrence of mixed planktic and benthic foraminifera specimens in core GeoB19905-1 (J. Weiser, pers. comm. 2021), which might correlate with the HTM-like conditions in the Middle Holocene (cf. Discussion for more explanation). I to III represent different environmental periods shown in the maps of Fig. 10, based on our proxy records.

For the Middle Holocene between 5.9–3.0 ka BP, i.e. after the hiatus, our records from core GeoB19905-1 off NE Labrador Sea show ice-free conditions in spring–autumn as displayed by the continued absence of ice algae biomarkers ($IP_{25} = 0$; Fig. 4J). Dinosterol accumulation rates show a slight increase in this interval (Fig. 8F); however, $CaCO_3$ accumulation rates remained rather high until about 4 ka BP (Fig. 8F, G), suggesting subsurface conditions characterized by high biological (carbonate) productivity. This interpretation is supported by the continuously maximum occurrence of mixed planktic and benthic foraminifera specimens in the same core GeoB19905-1 (Fig. 8). Based on dinocyst data in the nearby core SA13-ST3 (Fig. 5B), Allan *et al.* (2021) have reported the subsurface conditions as characterized by a slight decrease in (winter) SIC (<4 months per year) and a variably high summer primary productivity. Overall, this may indicate persistent warm subsurface conditions in this area corresponding to the final stage of the HTM. Moros *et al.* (2016) (core MSM343300) and Seidenkrantz *et al.* (2013) (core 248260-2) also suggested warm surface water conditions, in combination with low meltwater influx from the GIS in the eastern Baffin Bay area. Based on terrestrial evidence from SW Greenland and NE Canada a rather late HTM lasting until about 4.0 ka BP has been suggested (Fredskild, 1985a, b; Willemse & Tornqvist 1999; Kaplan *et al.* 2002; Moros *et al.* 2006). Based on the foraminifera records from offshore East Greenland, Jennings *et al.* (2002) described a strong influence of Atlantic Intermediate Water during the Middle Holocene lasting until about ~4 ka BP. In Ameralik Fjord (cores DA41P, 248260-2), close to our core site, relatively warm subsurface conditions linked to strong WGC influence have also been reported, in agreement with our study (Moller *et al.* 2006; Seidenkrantz *et al.* 2007). Furthermore, based on mean sortable silt (grain-size) data on the same core (GeoB19905-1), Weiser *et al.* (2021) showed a slight decrease in the WGC strength during the Middle Holocene (Fig. 8H); however, a large

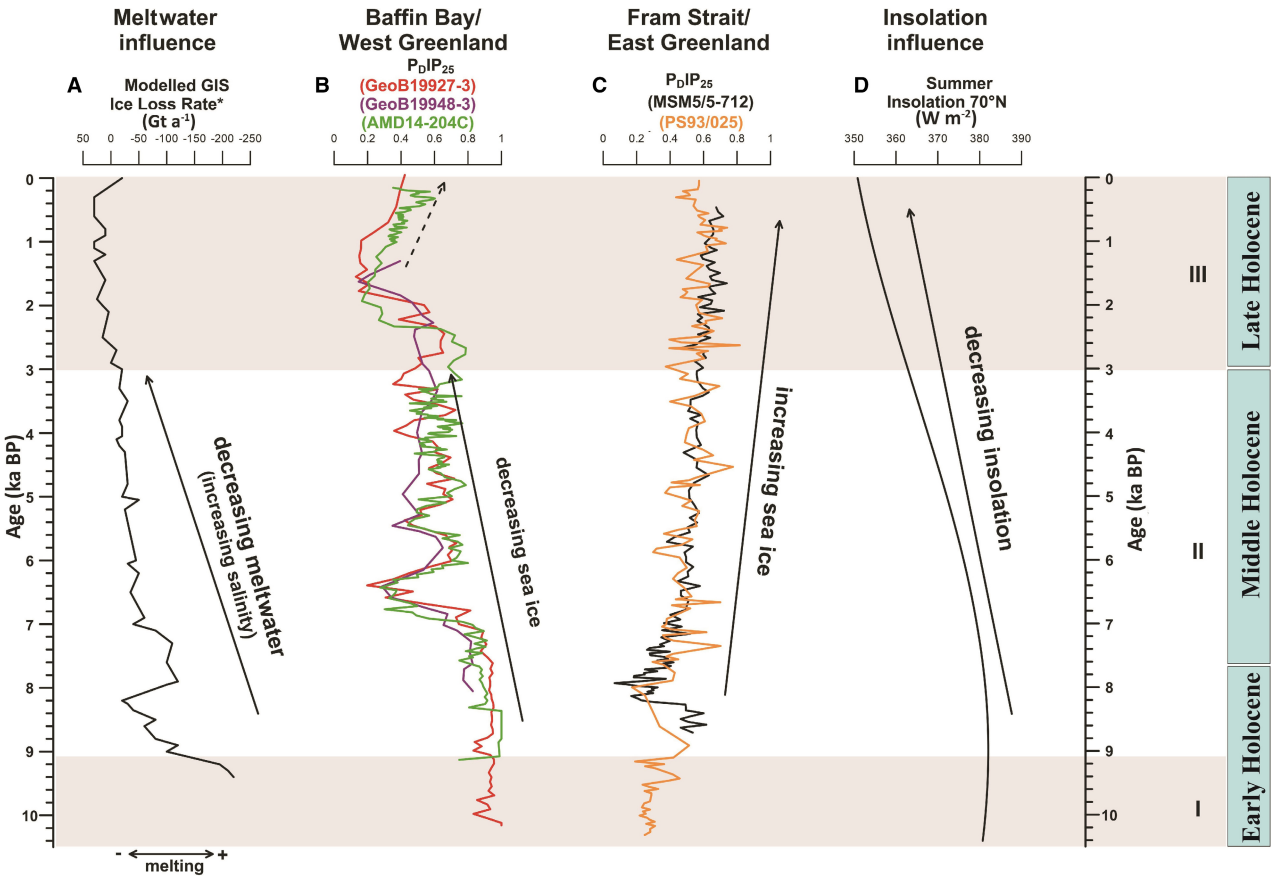

Fig. 9. Comparison and down-core variations of sea-ice conditions in Baffin Bay and Fram Strait area. A. Modelled GIS ice loss rate (Lecavalier *et al.* 2014). B. $P_{III}IP_{25}$ indices from cores GeoB19927-3 (Saini *et al.* 2020); GeoB19948-3; AMD14-204C (Limoges *et al.* 2020). C. P_DIP_{25} index; core MSM5/5-712 (Müller *et al.* 2012). D. Summer insolation at 70°N (Laskar *et al.* 2004).

decrease in the meltwater discharge along the SW Greenland margin in this interval (Holland *et al.* 2008; Ren *et al.* 2009; Gibb *et al.* 2015) may have substantially increased subsurface salinity, thus maintaining a strong influence of Atlantic Water (WGC) to the ocean surface. Biomarker proxies, including sediment composition (grain-size) data, have already been previously successfully applied for subsurface and bottom water conditions in the High Northern Latitude areas, i.e. Denmark Strait and Labrador Sea (Andrews *et al.* 2020; Weiser *et al.* 2021).

Towards the final stage of the Middle Holocene (~4–3 ka BP) at core site GeoB19905-1 in the Labrador Sea, the accumulation rates of $CaCO_3$ display a decrease whereas dinosterol accumulation rates remain unchanged (Fig. 8F, G). This suggests changes in subsurface conditions characterized by either a decrease in biological (carbonate) productivity and/or a decrease in preservation of organic carbon (i.e. $CaCO_3$ and TOC). $CaCO_3$ has been interpreted as productivity indicator very selectively as in core GeoB19905-1, J. Weiser (pers. comm. 2021) has analysed the foraminifera data showing well-preserved, mixed planktic and benthic specimens, coinciding with the increased $CaCO_3$ accumulation rates. This might suggest that the $CaCO_3$ is mainly of biogenic origin; hence, its accumulation rates could be used to infer surface and subsurface productivity. Here, this decrease in biological (carbonate) productivity could be linked to a decline in the WGC strengths, while the high dinosterol accumulation rates might be due to the increased deposition of fine-grained sediments (Fig. 8H; Weiser *et al.* 2021). The declined WGC strength temporally coincides with the onset of Neoglacial cooling, widely reported around Greenland areas (Levac *et al.* 2001; Long & Roberts 2003; Briner *et al.* 2010; Müller *et al.* 2012; Perner *et al.* 2012; Krawczyk *et al.* 2017; Schweinsberg *et al.* 2017). Dinocyst-based reconstructions in the nearby core SA13-ST3 also indicate a slight decrease in summer primary productivity in this interval (Allan *et al.* 2021), in agreement with our study. Moros *et al.* (2004) also argued for a period (4–3 ka BP) of climate instability and significant fluctuation in EGC and IC strengths in the East Greenland margin leading to cooling. Several lake sediment records in the vicinity of Southwest Greenland also showed renewed ice growth and enhanced glacier activity starting *c.* 4 ka BP (Larsen

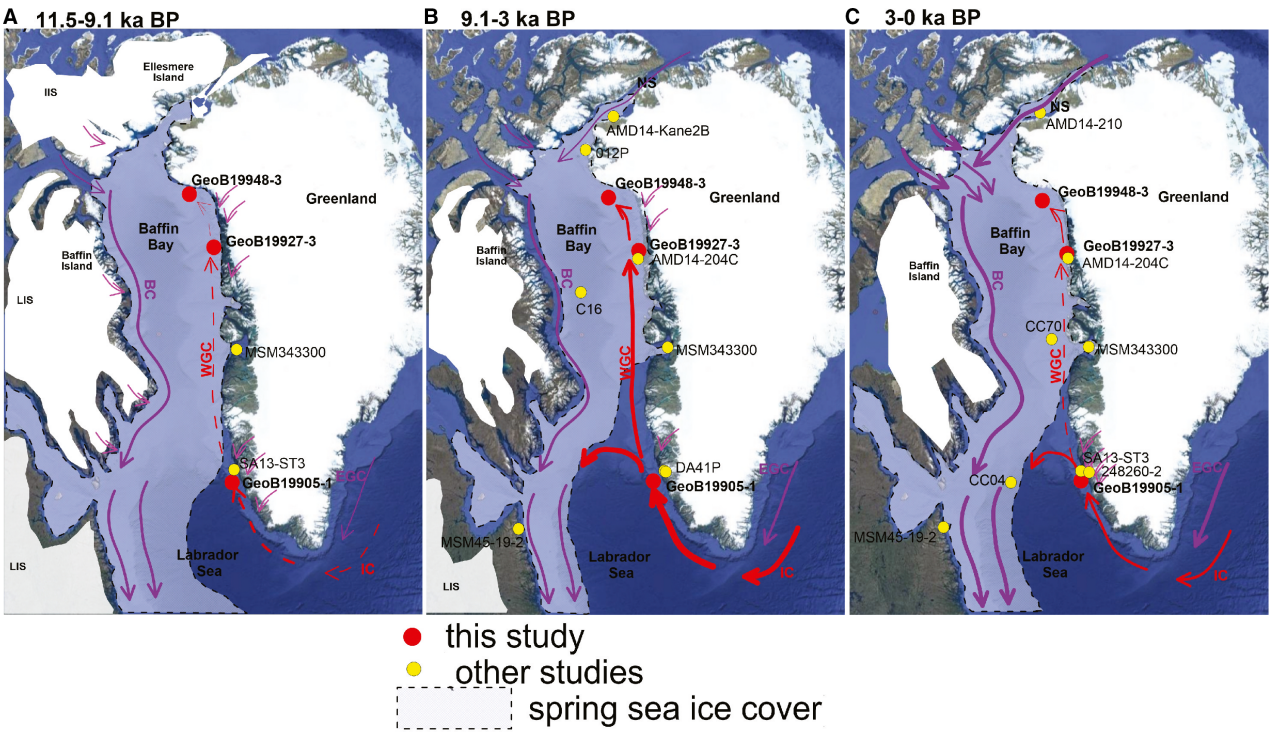

Fig. 10. Schematic oceanographic conditions in Baffin Bay and the Labrador Sea for three time intervals A–C during the Holocene from 11.5 ka to present based on this and previous studies from the area: core MSM343300 (Perner *et al.* 2012; Moros *et al.* 2016), core 012P (Levac *et al.* 2001; Knudsen *et al.* 2008), cores AMD14-204C, AMD14-210 and GeoB19927-3 from Melville Bugt (Caron *et al.* 2019; Hansen *et al.* 2020; Saini *et al.* 2020), core AMD14-Kane2B (Georgiadis *et al.* 2020), cores DA41P, SA13-ST3 and 248260-2 from NE Labrador Sea (Seidenkrantz 2013; Seidenkrantz *et al.* 2013; Allan *et al.* 2021), cores CC04 and CC70 (Gibb *et al.* 2015), and core MSM45-19-2 (Lochte *et al.* 2019). Red and Purple arrows indicate warmer and colder ocean currents whereas solid (or thick) and dashed (or thin) arrows indicate stronger or weaker current strengths, respectively. The magenta arrows indicate meltwater inflow to the core site.

et al. 2017), supporting the onset of Neoglacial cooling in this time interval.

Late Holocene changes in sea-surface conditions (3–0 ka BP)

Surface water cooling along the West Greenland coast during the Late Holocene Neoglacial period is attributed to the variability in the strength of the Atlantic (IC) vs. Arctic (EGC, BC) currents (Moros *et al.* 2006; Seidenkrantz *et al.* 2007; Andresen *et al.* 2011; Ouellet-Bernier *et al.* 2014). Interestingly, our sea ice (IP_{25}) and phytoplankton biomarkers (dinosterol, HBI III), and related $P_{III}IP_{25}$ indices display reduced values (Figs 3, S2), and low accumulation rates of all biomarkers during this period at core sites GeoB19948-3 and GeoB19927-3, which may be attributed to stratified conditions associated with an enhanced input of cold corrosive Polar Water (Fig. 10C) hampering productivity. Based on diatom and biomarker data from core AMD14-204C, Limoges *et al.* (2020) point towards major oceanographic reorganization that may be related to the strengthening of the EGC and/or decreased contribution of warm IC into the WGC (Flatau *et al.* 2003; Morley *et al.* 2014). Based on the increased abundance of agglutinated foraminifera species in cores AMD14-204C and MSM343300, Hansen *et al.* (2020) and Perner *et al.* (2012) suggested enhanced Arctic Water influx into Baffin Bay and strongly stratified conditions during the Late Holocene. Based on diatom assemblages from nearby core AMD14-204C, Limoges *et al.* (2020) also reported enhanced drift/pack-ice in this interval, which might have contributed to increased multi-year sea-ice (IP_{25}-poor) presence and decreased primary production in this area. High peaks in the HBI III records from cores GeoB19927-3, GeoB19948-3 and AMD14-204C (Figs 3, S2) in this interval suggest an extended sea ice cover, which further indicates increased (multi-year) sea ice in Baffin Bay imported via Nares Strait (Fig. 10C; Limoges *et al.* 2020; Saini *et al.* 2020). This is further supported by a decrease in winter snowfall in western Greenland areas (Thomas *et al.* 2016), implying a more extensive SIC that might have limited moisture availability during this interval. Afterwards, low to moderate $P_{III}IP_{25}$ values (0.2–0.6) between 1.8 and 1.2 ka BP at core sites GeoB19927-3 and GeoB19948-3 (Fig. 5) might indicate a short interval of reduced sea ice cover associated with a positive NAO mode and related warmer subsurface conditions in eastern Baffin Bay (Moros *et al.* 2006; Trouet *et al.* 2009; Andresen *et al.*

2011; Gibb *et al.* 2015). Increased SSTs were also suggested near the East Greenland shelves at *c.* 1.8–1.2 ka BP (Knudsen *et al.* 2004; Roncaglia & Kuijpers 2004). The reduction in SIC might be also attributed to strong sea-ice interactions with the local fjords, which can also hamper ice growth (Ribeiro *et al.* 2017) as a result of poor light availability due to higher snow conditions as well as low salinity levels resulting from high local meltwater runoff. The short-term warming in the North Atlantic and the in-phase relationship between sea ice and NAO mode have been previously reported (Trouet *et al.* 2009; Ljungqvist 2010; Limoges *et al.* 2020; Saini *et al.* 2020). An increasing trend in SIC is more clearly evidenced after about 1.4 ka BP as shown by $P_{III}IP_{25}$ indices in cores GeoB19927-3, GeoB19948-3 and AMD14-204C (Limoges *et al.* 2020; Fig. 5), coinciding with Neoglacial cooling observed elsewhere (Fig. 10C and references therein). Based on the increase in Arctic Water indicator dinocysts (*Islandinium minutum*; core AMD14-204C) during the last ~1.4 ka, Caron *et al.* (2019) have described an increase in SIC and colder conditions in eastern Baffin Bay related to Neoglacial cooling. Based on IP_{25} and diatom records from core AMD14-204C, Limoges *et al.* (2020) also suggested an increased SIC during the last 1.4 ka BP and colder Neoglacial conditions. This is further supported by enhanced driftwood findings during the Late Holocene in the Canadian Arctic Archipelago, possibly carried along by the strengthened Polar Water (i.e. BC) masses (Dyke *et al.* 1997). This increase in SIC during the Neoglacial period is in agreement with the reconstructions from the northern Baffin Bay (Levac *et al.* 2001) and the eastern Fram Strait area (Fig. 9) (Müller & Stein 2014; Syring *et al.* 2020).

However, in the NE Labrador Sea, after 3 ka BP, HTM-like conditions were followed by surface and subsurface conditions characterized by the absence of ice algae biomarkers and significantly decreased $CaCO_3$ accumulation rates (Fig. 4E, J), albeit very high accumulation of the phytoplankton biomarker dinosterol (Fig. 8F; core GeoB19905-1). Based on the end-member grain-size analysis of the same core (GeoB19905-1), Weiser *et al.* (2021) documented a strong increase in the accumulation of poorly-sorted fine-grained sediments (Fig. 8C) presumably from the Neoglacial ice-margin advances. Due to increased flocculation/coagulation of fine-grained siliciclastic material ('ballast effect'; cf. Ittekkot *et al.* 1992; Knies & Stein 1998; Fahl & Stein 2007; Iversen & Robert 2015), organic matter may become enriched in such finer-grained sediments as shown by elevated TOC values and high accumulation rates of organic carbon (Fig. 4). This may have resulted in more labile organic matter preservation in the sediments. Another explanation for the increased accumulation rates of the phytoplankton biomarkers in the Late Holocene (Fig. 8F) might be the increased nutrient supply (e.g. Fe, Si) associated with the enhanced local meltwater discharge (Bhatia *et al.* 2013; Hawkings *et al.* 2015; Arrigo *et al.* 2017; Cape *et al.* 2019). Based on exploration studies from the nearby Sinarsuk deposit, Secher (1980) and Grammatikopoulos *et al.* (2002) found a significant amount of magnetite in the host rock, which might be a potential source of high Fe contents recorded in the Late Holocene section of the core GeoB19905-1 (Weiser *et al.* 2021).

The last 0.4 ka (upper ~100 cm, core GeoB19905-1, Fig. 4) are characterized by very high phytoplankton biomarker accumulation rates that might be explained on one hand by increased phytoplankton productivity/increased preservation. On the other hand, the topmost maximum value and its down-core decrease may represent diagenetic alterations in the uppermost centimetres (cf. Fahl & Stein 2012; Belt & Müller 2013). The drop in phytoplankton biomarkers (Fig. 8F, G) evident at about 0.3 ka BP (*c.* AD 1700) may be correlated with the Little Ice Age (LIA), widely reported in the Western Europe and North Atlantic regions (Jones & Mann 2004; Ljungqvist 2010; Spielhagen *et al.* 2011). However, more high-resolution reconstructions are needed to resolve the decadal to centennial-scale climate events.

Conclusions

Organic geochemical and biomarker investigation of AMS ^{14}C-dated sediment cores (GeoB19948-3, GeoB19927-3, GeoB19905-1) from a N–S transect of the eastern Baffin Bay-Labrador Sea margin was used for environmental and palaeoceanographic reconstruction covering the Holocene period. Our data based on cores GeoB19948-3 and GeoB19927-3 suggest that Baffin Bay was seasonally covered by sea ice during the last ~10.1 ka. In contrast, predominantly ice-free (spring and/or autumn) conditions were observed during the last 11.5 ka in the NE Labrador Sea (core GeoB19905-1). We record a general decrease in SIC conditions along the N–S transect throughout the Holocene.

Extended (early) spring SIC conditions occurred prior to ~7.6 ka BP in the Early Holocene in eastern Baffin Bay, possibly linked to the limited subsurface presence of Atlantic Water (WGC). However, in the NE Labrador Sea, conditions remained mostly ice-free in spring–autumn in the Early Holocene due to the increasing but limited influence of Atlantic Water (WGC).

A transition towards decreased SIC and reoccurring ice-edge conditions is evident in the Middle Holocene (~7.6–3 ka BP), possibly caused by the short-term (cyclic) changes in the WGC influence associated with ice melting and can be characterized by HTM-like conditions. This decrease in SIC is synchronous with the decrease in the meltwater inflow leading to the salinization of surface waters in the Baffin Bay area. The HTM-like conditions in the Middle Holocene, in response to the final retreat of the LIS and GIS, are also recorded in the NE Labrador Sea, displayed by spring–autumn ice-free (PIP_{25} = 0) conditions together with an increased accumulation of productivity indicators.

Our combined sea-ice records from Baffin Bay indicate low *in-situ* sea-ice (IP_{25}) algae production; however, enhanced drifted (multi-year) sea ice during the Late Holocene (last 3 ka BP) associated with the enhanced influx of Polar Water masses might have caused stratified conditions resulting in reduced primary productivity related to the Neoglacial cooling trend observed elsewhere. However, in the NE Labrador Sea, surface conditions were characterized by (spring–autumn) ice-free conditions with a strong decrease in carbonate productivity during the last *c*. 4 ka, in line with decreased WGC strengths and/or enhanced advection of cold Arctic Water masses and increased meltwater inflow linked to the Neoglacial cooling. Our sea-ice records from the Baffin Bay-Labrador Sea on the West Greenland side indicate that meltwater input has mainly controlled sea-ice formation during the Holocene, in contrast to the East Greenland side (i.e. Fram Strait), where the Holocene sea-ice history follows predominantly the summer insolation trend.

Acknowledgements. – We would like to thank the captain, the science party and the crew of RV 'Maria S. Merian' MSM44 for their excellent work. We are thankful to Walter Luttmer and Susanti Wirda for technical support in the laboratory. We are also very thankful to Gesine Mollenhauer for high-precision analyses of small-scale ^{14}C samples with the AWI MICADAS facility. The financial support by the Deutsche Forschungsgemeinschaft through 'ArcTrain' (GRK 1904) is gratefully acknowledged. Furthermore, we would like to thank two anonymous reviewers and the editor for their helpful comments to improve this manuscript.

Author contributions. – JS, RS and KF conceptualized and designed the experiment. JS performed the preparation of samples (freeze-drying, grinding), the bulk organic-geochemical analyses (TOC, CNS) and the biomarker analyses (HBIs, sterols). LM performed the TOC, CNS analyses of core GeoB19948-3. JW performed the AMS^{14}C datings on cores GeoB19948-3, GeoB19927-3 and GeoB19905-1. KF performed quality control of the biomarkers. JS performed the interpretation of the results and wrote the first versions of the manuscript with support and input of RS. RS, KF, JW and DH supported the interpretation of results and improvements on the manuscript. All authors reviewed the results and approved the final version of the manuscript with no known conflict of interests.

References

Aksenov, Y., Bacon, S., Coward, A. C. & Holliday, N. P. 2010: Polar outflow from the Arctic Ocean: a high resolution model study. *Journal of Marine Systems 83*, 14–37.

Allan, E., de Vernal, A., Seidenkrantz, M.-S., Briner, J. P., Hillaire-Marcel, C., Pearce, C., Meire, L., Røy, H., Mathiasen, A. M., Nielsen, M. T., Plesner, J. L. & Perner, K. 2021: Insolation vs. meltwater control of productivity and sea surface conditions off SW Greenland during the Holocene. *Boreas 50*, 631–651.

Andresen, C. S., McCarthy, D. J., Dylmer, C. V., Seidenkrantz, M.-S., Kuijpers, A. & Lloyd, J. M. 2011: Interaction between subsurface ocean waters and calving of the Jakobshavn Isbrae during the late Holocene. *The Holocene 21*, 211–224.

Andrews, J. T., Keigwin, L., Hall, F. & Jennings, A. E. 1999: Abrupt deglaciation events and Holocene palaeoceanography from high-resolution cores, Cartwright Saddle, Labrador Shelf, Canada. *Journal of Quaternary Science 14*, 383–397.

Andrews, J. T., Smik, L., Belt, S. T., Sicre, M. A. & McCave, I. N. 2020: Ocean surface and bottom water conditions, iceberg drift and sediment transport on the North Iceland margin during MIS 3 and MIS 2. *Quaternary Science Reviews 252*, 106722, https://doi.org/10.1016/j.quascirev.2020.106722.

Arrigo, K. R., van Dijken, G. L., Castelao, R. M., Luo, H., Rennermalm, A. K., Tedesco, M., Mote, T. L., Oliver, H. & Yager, P. L. 2017: Melting glaciers stimulate large summer phytoplankton blooms in southwest Greenland waters. *Geophysical Research Letters 44*, 6278–6285.

Belt, S. T. 2018: Source-specific biomarkers as proxies for Arctic and Antarctic sea ice. *Organic Geochemistry 125*, 277–298.

Belt, S. T. & Müller, J. 2013: The Arctic sea ice biomarker IP25: a review of current understanding, recommendations for future research and applications in palaeo sea ice reconstructions. *Quaternary Science Reviews 79*, 9–25.

Belt, S. T., Cabedo-Sanz, P., Smik, L., Navarro-Rodriguez, A., Berben, S. M. P., Knies, J. & Husum, K. 2015: Identification of paleo Arctic winter sea ice limits and the marginal ice zone: optimised biomarker-based reconstructions of late Quaternary Arctic sea ice. *Earth and Planetary Science Letters 431*, 127–139.

Belt, S. T., Masse, G., Rowland, S. J., Poulin, M., Michel, C. & LeBlanc, B. 2007: A novel chemical fossil of palaeo sea ice: IP25. *Organic Geochemistry 38*, 16–27.

Belt, S. T., Smik, L., Köseoğlu, D., Knies, J. & Husum, K. 2019: A novel biomarker-based proxy for the spring phytoplankton bloom in Arctic and sub-arctic settings - HBI T-25. *Earth and Planetary Science Letters 523*, 11, https://doi.org/10.1016/j.epsl.2019.06.038.

Bhatia, M. P., Kujawinski, E. B., Das, S. B., Breier, C. F., Henderson, P. B. & Charette, M. A. 2013: Greenland meltwater as a significant and potentially bioavailable source of iron to the ocean. *Nature Geoscience 6*, 274–278.

Bhatt, U. S., Walker, D. A., Walsh, J. E., Carmack, E. C., Frey, K. E., Meier, W. N., Moore, S. E., Parmentier, F.-J.-W., Post, E., Romanovsky, V. E. & Simpson, W. R. 2014: Implications of Arctic sea ice decline for the Earth system. *Annual Review of Environment and Resources 39*, 57–89.

Blaauw, M. & Christen, J. A. 2011: Flexible paleoclimate age-depth models using an autoregressive gamma process. *Bayesian Analysis 6*, 457–474.

Boon, J. J., Rijpstra, W. I. C., Delange, F., Deleeuw, J. W., Yoshioka, M. & Shimizu, Y. 1979: Black Sea sterol - molecular fossil for dinoflagellate blooms. *Nature 277*, 125–127.

Briner, J. P., Hakansson, L. & Bennike, O. 2013: The deglaciation and neoglaciation of Upernavik Isstrom, Greenland. *Quaternary Research 80*, 459–467.

Briner, J. P., McKay, N. P., Axford, Y., Bennike, O., Bradley, R. S., de Vernal, A., Fisher, D., Francus, P., Frechette, B., Gajewski, K., Jennings, A., Kaufman, D. S., Miller, G., Rouston, C. & Wagner, B. 2016: Holocene climate change in Arctic Canada and Greenland. *Quaternary Science Reviews 147*, 340–364.

Briner, J. P., Stewart, H. A. M., Young, N. E., Philipps, W. & Losee, S. 2010: Using proglacial-threshold lakes to constrain fluctuations of the Jakobshavn Isbrae ice margin, western Greenland, during the Holocene. *Quaternary Science Reviews 29*, 3861–3874.

Brown, T. A. & Belt, S. T. 2016: Novel tri- and tetra-unsaturated highly branched isoprenoid (HBI) alkenes from the marine diatom Pleurosigma intermedium. *Organic Geochemistry 91*, 120–122.

Bunker, A. F. 1976: Computations of surface energy flux and annual air-sea interaction cycles of the North Atlantic Ocean. *Monthly Weather Review 104*, 1122–1140.

Butzin, M., Köhler, P. & Lohmann, G. 2017: Marine radiocarbon reservoir age simulations for the past 50,000 years. *Geophysical Research Letters 44*, 8473–8480.

Cape, M. R., Straneo, F., Beaird, N., Bundy, R. M. & Charette, M. A. 2019: Nutrient release to oceans from buoyancy-driven upwelling at Greenland tidewater glaciers. *Nature Geoscience 12*, 34–39.

Caron, M., Rochon, A., Montero-Serrano, J. C. & St-Onge, G. 2019: Evolution of sea-surface conditions on the northwestern Greenland margin during the Holocene. *Journal of Quaternary Science 34*, 569–580.

Dieckmann, G. S. & Hellmer, H. H. 2003: The importance of sea ice: an overview. *In* Thomas, D. N. & Dieckmann, G. S. (eds.): *Sea Ice: An Introduction to Its Physics, Chemistry, Biology and Geology*, 1–22. Blackwell Science Ltd, Oxford.

Dorschel, B., Gebhardt, A. C., Hebbeln, D., & Sichha, M. 2015: *BAFFEAST Past Greenland Ice Sheet Dynamics, Palaeoceanography and Plankton Ecology in the Northeast Baffin Bay*. Cruise No. MSM44 - June 30–July 30, 2015 - Nuuk (Greenland) - Nuuk (Greenland), MARIA S. MERIAN. Alfred-Wegener-Institute.

Dyke, A. S., England, J., Reimnitz, E. & Jette, H. 1997: Changes in driftwood delivery to the Canadian Arctic Archipelago: the hypothesis of postglacial oscillations of the Transpolar Drift. *Arctic 50*, 1–16.

Dyke, A. S., Hooper, J. & Savelle, J. M. 1996: A history of sea ice in the Canadian Arctic Archipelago based on postglacial remains of the bowhead whale (Balaena mysticetus). *Arctic 49*, 235–255.

Fahl, K. & Stein, R. 2007: Biomarker records, organic carbon accumulation, and river discharge in the Holocene southern Kara Sea (Arctic Ocean). *Geo-Marine Letters 27*, 13–25.

Fahl, K. & Stein, R. 2012: Modern seasonal variability and deglacial/Holocene change of central Arctic Ocean sea-ice cover: new insights from biomarker proxy records. *Earth and Planetary Science Letters 351*, 123–133.

Flatau, M. K., Talley, L. & Niiler, P. P. 2003: The North Atlantic Oscillation, surface current velocities, and SST changes in the subpolar North Atlantic. *Journal of Climate 16*, 2355–2369.

Fredskild, B. 1985a: Holocene pollen records from West Greenland. *In* Andrews, J. T. (ed.): *Quaternary Environments, Eastern Canadian Arctic, Baffin Bay and Western Greenland*, 643–681. Allen and Unwin, Boston.

Fredskild, B. 1985b: The Holocene vegetational development of Tugtuligssuaq and Qeqertat, Northwest Greenland. *Meddelelser om Grønland, Geoscience 14*, 1–20.

Georgiadis, E., Giraudeau, J., Jennings, A., Limoges, A., Jackson, R., Ribeiro, S. & Massé, G. 2020: Local and regional controls on Holocene sea ice dynamics and oceanography in Nares Strait, Northwest Greenland. *Marine Geology 422*, 106115, https://doi.org/10.1016/j.margeo.2020.106115.

Georgiadis, E., Giraudeau, J., Martinez, P., Lajeunesse, P., St-Onge, G., Schmidt, S. & Masse, G. 2018: Deglacial to postglacial history of Nares Strait, Northwest Greenland: a marine perspective from Kane Basin. *Climate of the Past 14*, 1991–2010.

Gersonde, R., Crosta, X., Abelmann, A. & Armand, L. 2005: Sea-surface temperature and sea ice distribution of the Southern Ocean at the EPILOG Last Glacial Maximum - a circum-Antarctic view based on siliceous microfossil records. *Quaternary Science Reviews 24*, 869–896.

Gibb, O. T., Steinhauer, S., Fréchette, B., de Vernal, A. & Hillaire-Marcel, C. 2015: Diachronous evolution of sea surface conditions in the Labrador Sea and Baffin Bay since the last deglaciation. *The Holocene 25*, 1882–1897.

Grammatikopoulos, T., McKen, A., Hamilton, C. & Christiansen, O. 2002: Vanadium-bearing magnetite and ilmenite mineralization and beneficiation from the Sinarsuk V-Ti project, West Greenland. *Cim Bulletin 95*, 87–95.

Hansen, K. E., Giraudeau, J., Wacker, L., Pearce, C. & Seidenkrantz, M.-S. 2020: Reconstruction of Holocene oceanographic conditions in the Northeastern Baffin Bay. *Climate of the Past 3*, 1075–1095.

Hawkings, J. R., Wadham, J. L., Tranter, M., Lawson, E., Sole, A., Cowton, T., Tedstone, A. J., Bartholomew, I., Nienow, P., Chandler, D. & Telling, J. 2015: The effect of warming climate on nutrient and solute export from the Greenland Ice Sheet. *Geochemical Perspectives Letters 1*, 94–104.

Hillaire-Marcel, C. & de Vernal, A. 2008: Stable isotope clue to episodic sea ice formation in the glacial North Atlantic. *Earth and Planetary Science Letters 268*, 143–150.

Holland, D. M., Thomas, R. H., De Young, B., Ribergaard, M. H. & Lyberth, B. 2008: Acceleration of Jakobshavn Isbrae triggered by warm subsurface ocean waters. *Nature Geoscience 1*, 659–664.

Ittekkot, V., Haake, B., Bartsch, M., Nair, R. R. & Ramaswamy, V. 1992: Organic carbon removal in the sea: the continental connection. *Geological Society, London, Special Publications 64*, 167–176.

Iversen, M. H. & Robert, M. L. 2015: Ballasting effects of smectite on aggregate formation and export from a natural plankton community. *Marine Chemistry 175*, 18–27.

Jakobsson, M., Long, A., Ingolfsson, O., Kjaer, K. H. & Spielhagen, R. F. 2010: New insights on Arctic Quaternary climate variability from palaeo-records and numerical modelling. *Quaternary Science Reviews 29*, 3349–3358.

Jennings, A. E. 1993: The Quaternary history of Cumberland Sound, southeastern Baffin-Island - the marine evidence. *Geographie physique et Quaternaire 47*, 21–42.

Jennings, A. E., Andrews, J. T., Oliver, B., Walczak, M. & Mix, A. 2019: Retreat of the Smith Sound Ice Stream in the Early Holocene. *Boreas 48*, 825–840.

Jennings, A., Andrews, J. & Wilson, L. 2011: Holocene environmental evolution of the SE Greenland Shelf north and south of the Denmark Strait: Irminger and East Greenland current interactions. *Quaternary Science Reviews 30*, 980–998.

Jennings, A. E., Knudsen, K. L., Hald, M., Hansen, C. V. & Andrews, J. T. 2002: A mid-Holocene shift in Arctic sea-ice variability on the East Greenland Shelf. *The Holocene 12*, 49–58.

Jennings, A. E., Walton, M. E., Cofaigh, C. O., Kilfeather, A., Andrews, J. T., Ortiz, J. D., De Vernal, A. & Dowdeswell, J. A. 2014: Paleoenvironments during Younger Dryas-Early Holocene retreat of the Greenland Ice Sheet from outer Disko Trough, central west Greenland. *Journal of Quaternary Science 29*, 27–40.

Jones, P. D. & Mann, M. E. 2004: Climate over past millennia. *Reviews of Geophysics 42*, RG2002, https://doi.org/10.1029/2003RG000143.

Justwan, A., Koç, N. & Jennings, A. E. 2008: Evolution of the Irminger and East Icelandic Current systems through the Holocene, revealed by diatom-based sea surface temperature reconstructions. *Quaternary Science Reviews 27*, 1571–1582.

Kaplan, M. R., Wolfe, A. P. & Miller, G. H. 2002: Holocene environmental variability in southern Greenland inferred from lake sediments. *Quaternary Research 58*, 149–159.

Kaufman, D. S., Ager, T. A., Anderson, N. J., Anderson, P. M., Andrews, J. T., Bartlein, P. J., Brubaker, L. B., Coats, L. L., Cwynar, L. C., Duvall, M. L., Dyke, A. S., Edwards, M. E., Eisner, W. R., Gajewski, K., Geirsdottir, A., Hu, F. S., Jennings, A. E., Kaplan, M. R., Kerwin, M. N., Lozhkin, A. V., MacDonald, G. M., Miller, G. H., Mock, C. J., Oswald, W. W., Otto-Bliesner, B. L., Porinchu, D. F., Ruhland, K., Smol, J. P., Steig, E. J. & Wolfe, B. B. 2004: Holocene thermal maximum in the western Arctic (0–180 degrees W). *Quaternary Science Reviews 23*, 529–560.

Kinnard, C., Zdanowicz, C. M., Fisher, D. A., Isaksson, E., de Vernal, A. & Thompson, L. G. 2011: Reconstructed changes in Arctic sea ice over the past 1,450 years. *Nature 479*, 509–512.

Knies, J. & Stein, R. 1998: New aspects of organic carbon deposition and its paleoceanographic implications along the northern Barents Sea margin during the last 30,000 years. *Paleoceanography 13*, 384–394.

Knudsen, K. L., Jiang, H., Jansen, E., Eiriksson, J., Heinemeier, J. & Seidenkrantz, M.-S. 2004: Environmental changes off North Iceland during the deglaciation and the Holocene: foraminifera, diatoms and stable isotopes. *Marine Micropaleontology 50*, 273–305.

Knudsen, K. L., Stabell, B., Seidenkrantz, M.-S., Eiriksson, J. & Blake, W. 2008: Deglacial and Holocene conditions in northernmost Baffin Bay: sediments, foraminifera, diatoms and stable isotopes. *Boreas 37*, 346–376.

Kolling, H. M., Stein, R., Fahl, K., Perner, K. & Moros, M. 2018: New insights into sea ice changes over the past 2.2 kyr in Disko Bugt, West Greenland. *Arktos 4*, 11, https://doi.org/10.1007/s41063-018-0045-z.

Kolling, H. M., Stein, R., Fahl, K., Sadatzki, H., de Vernal, A. & Xiao, X. 2020: Biomarker distributions in (sub)-Arctic surface sediments and their potential for sea-ice reconstructions. *Geochemistry, Geophysics, Geosystems 21*, e2019GC008629, https://doi.org/10.1029/2019GC008629.

Krawczyk, D. W., Witkowski, A., Moros, M., Lloyd, J. M., Høyer, J. L., Miettinen, A. & Kuijpers, A. 2017: Quantitative reconstruction of Holocene sea ice and sea surface temperature off West Greenland from the first regional diatom data set. *Paleoceanography 32*, 18–40.

Langner, M. & Mulitza, S. 2019: Technical note: PaleoDataView – a software toolbox for the collection, homogenization and visualization of marine proxy data. *Climate of the Past 15*, 2067–2072.

Larsen, N. K., Strunk, A., Levy, L. B., Olsen, J., Bjørk, A., Lauridsen, T. L., Jeppesen, E. & Davidson, T. A. 2017: Strong altitudinal control on the response of local glaciers to Holocene climate change in southwest Greenland. *Quaternary Science Reviews 168*, 69–78.

Laskar, J., Robutel, P., Joutel, F., Gastineau, M., Correia, A. C. M. & Levrard, B. 2004: A long-term numerical solution for the insolation quantities of the Earth. *Astronomy & Astrophysics 428*, 261–285.

Lecavalier, B. S., Milne, G. A., Simpson, M. J. R., Wake, L., Huybrechts, P., Tarasov, L., Kjeldsen, K. K., Funder, S., Long, A. J., Woodroffe, S., Dyke, A. S. & Larsen, N. K. 2014: A model of Greenland ice sheet deglaciation constrained by observations of relative sea level and ice extent. *Quaternary Science Reviews 102*, 54–84.

Levac, E., De Vernal, A. & Blake, W. 2001: Sea-surface conditions in northernmost Baffin Bay during the Holocene: palynological evidence. *Journal of Quaternary Science 16*, 353–363.

Limoges, A., Weckström, K., Ribeiro, S., Georgiadis, E., Hansen, K. E., Martinez, P., Seidenkrantz, M.-S., Giraudeau, J., Crosta, X. & Massé, G. 2020: Learning from the past: Impact of the Arctic Oscillation on sea ice and marine productivity off northwest Greenland over the last 9,000 years. *Global Change Biology 26*, 6767–6786.

Ljungqvist, F. C. 2010: A new reconstruction of temperature variability in the extra-Tropical Northern Hemisphere during the last two millennia. *Geografiska Annaler Series A-Physical Geography 92A*, 339–351.

Lloyd, J. M., Park, L. A., Kuijpers, B. & Moros, M. 2005: Early Holocene palaeoceanography and deglacial chronology of Disko Bugt, West Greenland. *Quaternary Science Reviews 24*, 1741–1755.

Lochte, A. A., Repschlager, J., Seidenkrantz, M.-S., Kienast, M., Blanz, T. & Schneider, R. R. 2019: Holocene water mass changes in the Labrador Current. *The Holocene 29*, 676–690.

Long, A. J. & Roberts, D. H. 2003: Late Weichselian deglacial history of Disko Bugt, West Greenland, and the dynamics of the Jakobshavns Isbrae ice stream. *Boreas 32*, 208–226.

Manabe, S., Spelman, M. J. & Stouffer, R. J. 1992: Transient responses of a coupled ocean atmosphere model to gradual changes of atmospheric CO_2. Seasonal response. *Journal of Climate 5*, 105–126.

McPhee, M. G., Proshutinsky, A., Morison, J. H., Steele, M. & Alkire, M. B. 2009: Rapid change in freshwater content of the Arctic Ocean. *Geophysical Research Letters 36*, L10602, https://doi.org/10.1029/2009GL037525.

Moller, H. S., Jensen, K. G., Kuijpers, A., Aagaard-Sorensen, S., Seidenkrantz, M.-S., Prins, M., Endler, R. & Mikkelsen, N. 2006: Late-Holocene environment and climatic changes in Ameralik Fjord, southwest Greenland: evidence from the sedimentary record. *The Holocene 16*, 685–695.

Morison, J., Kwok, R., Peralta-Ferriz, C., Alkire, M., Rigor, I., Andersen, R. & Steele, M. 2012: Changing Arctic Ocean freshwater pathways. *Nature 481*, 66–70.

Morley, A., Rosenthal, Y. & deMenocal, P. 2014: Ocean-atmosphere climate shift during the mid-to-late Holocene transition. *Earth and Planetary Science Letters 388*, 18–26.

Moros, M., Emeis, K., Risebrobakken, B., Snowball, I., Kuijpers, A., McManus, J. & Jansen, E. 2004: Sea surface temperatures and ice rafting in the Holocene North Atlantic: climate influences on Northern Europe and Greenland. *Quaternary Science Reviews 23*, 2113–2126.

Moros, M., Jensen, K. G. & Kuijpers, A. 2006: Mid- to late-Holocene hydrological and climatic variability in Disko Bugt, central West Greenland. *The Holocene 16*, 357–367.

Moros, M., Lloyd, J. M., Perner, K., Krawczyk, D., Blanz, T., de Vernal, A., Ouellet-Bernier, M. M., Kuijpers, A., Jennings, A. E., Witkowski, A., Schneider, R. & Jansen, E. 2016: Surface and sub-surface multiproxy reconstruction of middle to late Holocene palaeoceanographic changes in Disko Bugt, West Greenland. *Quaternary Science Reviews 132*, 146–160.

Müller, J. & Stein, R. 2014: High-resolution record of late glacial and deglacial sea ice changes in Fram Strait corroborates ice-ocean interactions during abrupt climate shifts. *Earth and Planetary Science Letters 403*, 446–455.

Müller, J., Wagner, A., Fahl, K., Stein, R., Prange, M. & Lohmann, G. 2011: Towards quantitative sea ice reconstructions in the northern North Atlantic: a combined biomarker and numerical modelling approach. *Earth and Planetary Science Letters 306*, 137–148.

Müller, J., Werner, K., Stein, R., Fahl, K., Moros, M. & Jansen, E. 2012: Holocene cooling culminates in sea ice oscillations in Fram Strait. *Quaternary Science Reviews 47*, 1–14.

NSIDC 2012: *National Snow and Ice Data Center – Arctic Sea Ice News and Analysis*. http://nsidc.org/arcticseaicenews/.

NSIDC 2020: *National Snow and Ice Data Center – Arctic Sea Ice News and Analysis*. http://nsidc.org/arcticseaicenews/.

Ouellet-Bernier, M. M., de Vernal, A., Hillaire-Marcel, C. & Moros, M. 2014: Paleoceanographic changes in the Disko Bugt area, West Greenland, during the Holocene. *The Holocene 24*, 1573–1583.

Perner, K., Moros, M., Jennings, A., Lloyd, J. M. & Knudsen, K. L. 2012: Holocene palaeoceanographic evolution off West Greenland. *The Holocene 23*, 374–387.

Polyak, L., Alley, R. B., Andrews, J. T., Brigham-Grette, J., Cronin, T. M., Darby, D. A., Dyke, A. S., Fitzpatrick, J. J., Funder, S., Holland, M., Jennings, A. E., Miller, G. H., O'Regan, M., Savelle, J., Serreze, M., St. John, K., White, J. W. C. & Wolff, E. 2010: History of sea ice in the Arctic. *Quaternary Science Reviews 29*, 1757–1778.

Reimer, P. J., Bard, E., Bayliss, A., Beck, J. W., Blackwell, P. G., Ramsey, C. B., Buck, C. E., Cheng, H., Edwards, R. L., Friedrich, M., Grootes, P. M., Guilderson, T. P., Haflidason, H., Hajdas, I., Hatte, C., Heaton, T. J., Hoffmann, D. L., Hogg, A. G., Hughen, K. A., Kaiser, K. F., Kromer, B., Manning, S. W., Niu, M., Reimer, R. W., Richards, D. A., Scott, E. M., Southon, J. R., Staff, R. A., Turney, C. S. M. & van der Plicht, J. 2013: INTCAL13 and Marine13 radiocarbon age calibration curves 0–50,000 years cal BP. *Radiocarbon 55*, 1869–1887.

Ren, J., Jiang, H., Seidenkrantz, M.-S. & Kuijpers, A. 2009: A diatom-based reconstruction of Early Holocene hydrographic and climatic change in a southwest Greenland fjord. *Marine Micropaleontology 70*, 166–176.

Renssen, H., Seppä, H., Crosta, X., Goosse, H. & Roche, D. M. 2012: Global characterization of the Holocene Thermal Maximum. *Quaternary Science Reviews 48*, 7–19.

Ribeiro, S., Sejr, M. K., Limoges, A., Heikkilä, M., Andersen, T. J., Tallberg, P., Weckström, K., Husum, K., Forwick, M., Dalsgaard, T., Massé, G., Seidenkrantz, M.-S. & Rysgaard, S. 2017: Sea ice and primary production proxies in surface sediments from a High Arctic Greenland fjord: spatial distribution and implications for palaeoenvironmental studies. *Ambio 46*, S106–S118.

Ribergaard, M. H., Olsen, S. M. & Mortensen, J. 2008: Oceanographic Investigations off West Greenland 2007. Scientific Council Meeting, June 2008, NAFO SCR Doc. 08/3. https://archive.nafo.int/open/sc/2008/scr08-003.pdf.

Roncaglia, L. & Kuijpers, A. 2004: Palynofacies analysis and organic-walled dinoflagellate cysts in late-Holocene sediments from Igaliku Fjord, South Greenland. *The Holocene 14*, 172–184.

Saini, J., Stein, R., Fahl, K., Weiser, J., Hebbeln, D., Hillaire-Marcel, C. & de Vernal, A. 2020: Holocene variability in sea ice and primary productivity in the Northeastern Baffin Bay. *Arktos 6*, 55–73.

Sakshaug, E. 2004: Primary and secondary production in the Arctic seas. *In* Stein, R. & Macdonald, R. W. (eds.): *The Organic Carbon Cycle in the Arctic Ocean*, 57–82, Springer, Berlin.

Schweinsberg, A. D., Briner, J. P., Miller, G. H., Bennike, O. & Thomas, E. K. 2017: Local glaciation in West Greenland linked to North Atlantic Ocean circulation during the Holocene. *Geology 45*, 195–198.

Screen, J. A. & Simmonds, I. 2010: The central role of diminishing sea ice in recent Arctic temperature amplification. *Nature 464*, 1334–1337.

Secher, K. 1980: Distribution of radioactive mineralisation in central West Greenland. *Rapport Grønlands Geologiske Undersøgelse 100*, 61–65.

Seidenkrantz, M.-S. 2013: Benthic foraminifera as palaeo sea-ice indicators in the subarctic realm - examples from the Labrador Sea-Baffin Bay region. *Quaternary Science Reviews 79*, 135–144.

Seidenkrantz, M.-S., Aagaard-Sorensen, S., Sulsbruck, H., Kuijpers, A., Jensen, K. G. & Kunzendorf, H. 2007: Hydrography and climate of the last 4400 years in a SW Greenland fjord: implications for Labrador Sea palaeoceanography. *The Holocene 17*, 387–401.

Seidenkrantz, M.-S., Ebbesen, H., Aagaard-Sorensen, S., Moros, M., Lloyd, J. M., Olsen, J., Knudsen, M. F. & Kuijpers, A. 2013: Early Holocene large-scale meltwater discharge from Greenland documented by foraminifera and sediment parameters. *Palaeogeography, Palaeoclimatology, Palaeoecology 391*, 71–81.

Serreze, M. C. & Stroeve, J. 2015: Arctic sea ice trends, variability and implications for seasonal ice forecasting. *Philosophical Transactions of the Royal Society a-Mathematical Physical and Engineering Sciences 373*, 20140159, https://doi.org/10.1098/rsta.2014.0159.

Serreze, M. C., Barrett, A. P., Slater, A. G., Woodgate, R. A., Aagaard, K., Lammers, R. B., Steele, M., Moritz, R., Meredith, M. & Lee, C. M. 2006: The large-scale freshwater cycle of the Arctic. *Journal of Geophysical Research: Oceans 111*, C11010, https://doi.org/10.1029/2005JC003424.

Smik, L., Cabedo-Sanz, P. & Belt, S. T. 2016: Semi-quantitative estimates of paleo Arctic sea ice concentration based on source-specific highly branched isoprenoid alkenes: a further development of the PIP25 index. *Organic Geochemistry 92*, 63–69.

Spielhagen, R. F., Werner, K., Sorensen, S. A., Zamelczyk, K., Kandiano, E., Budeus, G., Husum, K., Marchitto, T. M. & Hald, M. 2011: Enhanced modern heat transfer to the Arctic by warm Atlantic water. *Science 331*, 450–453.

Stein, R. & Macdonald, R. W. 2004: Geochemical proxies used for organic carbon source identification in Arctic Ocean sediments. *In* Stein, R. & Macdonald, R. W. (eds.): *The Organic Carbon Cycle in the Arctic Ocean*, 24–32. Springer-Verlag, Berlin.

Syring, N., Stein, R., Fahl, K., Vahlenkamp, M., Zehnich, M., Spielhagen, R. F. & Niessen, F. 2020: Holocene changes in sea-ice cover and polynya formation along the eastern North Greenland shelf: New insights from biomarker records. *Quaternary Science Reviews 231*, 106173, https://doi.org/10.1016/j.quascirev.2020.106173.

Tang, C. C. L., Ross, C. K., Yao, T., Petrie, B., DeTracey, B. M. & Dunlap, E. 2004: The circulation, water masses and sea-ice of Baffin Bay. *Progress in Oceanography 63*, 183–228.

Thomas, E. K., Briner, J. P., Ryan-Henry, J. J. & Huang, Y. 2016: A major increase in winter snowfall during the middle Holocene on western Greenland caused by reduced sea ice in Baffin Bay and the Labrador Sea. *Geophysical Research Letters 43*, 5302–5308.

Thomas, D. N. & Dieckmann, G. S. 2010: *Sea Ice*. 621 pp. Blackwell Publishing, Oxford.

Trouet, V., Esper, J., Graham, N. E., Baker, A., Scourse, J. D. & Frank, D. C. 2009: Persistent positive North Atlantic Oscillation mode dominated the Medieval Climate Anomaly. *Science 324*, 78–80.

de Vernal, A., Gersonde, R., Goosse, H., Seidenkrantz, M.-S. & Wolff, E. W. 2013a: Sea ice in the paleoclimate system: the challenge of reconstructing sea ice from proxies - an introduction. *Quaternary Science Reviews 79*, 1–8.

de Vernal, A., Rochon, A., Frechette, B., Henry, M., Radi, T. & Solignac, S. 2013b: Reconstructing past sea ice cover of the Northern Hemisphere from dinocyst assemblages: status of the approach. *Quaternary Science Reviews 79*, 122–134.

Vinther, B. M., Buchardt, S. L., Clausen, H. B., Dahl-Jensen, D., Johnsen, S. J., Fisher, D. A., Koerner, R. M., Raynaud, D., Lipenkov, V., Andersen, K. K., Blunier, T., Rasmussen, S. O., Steffensen, J. P. & Svensson, A. M. 2009: Holocene thinning of the Greenland ice sheet. *Nature 461*, 385–388.

Volkman, J. K. 1986: A review of sterol markers for marine and terrigenous organic matter. *Organic Geochemistry 9*, 83–99.

Wacker, L., Fueloep, R. H., Hajdas, I., Molnar, M. & Rethemeyer, J. 2013: A novel approach to process carbonate samples for radiocarbon measurements with helium carrier gas. *Nuclear Instruments & Methods in Physics Research Section B-Beam Interactions with Materials and Atoms 294*, 214–217.

Wang, J., Mysak, L. A. & Ingram, R. G. 1994: Interannual variability of sea-ice cover in Hudson Bay, Baffin Bay and the Labrador Sea. *Atmosphere-Ocean 32*, 421–447.

Wassmann, P., Carmack, E. C., Bluhm, B. A., Duarte, C. M., Berge, J., Brown, K., Grebmeier, J. M., Holding, J., Kosobokova, K., Kwok, R., Matrai, P., Agusti, S., Babin, M., Bhatt, U., Eicken, H., Polyakov, I., Rysgaard, S. & Huntington, H. P. 2020: Towards a unifying pan-arctic perspective: a conceptual modelling toolkit. *Progress in Oceanography 189*, 102455, https://doi.org/10.1016/j.pocean.2020.102455.

Weiser, J., Titschack, J., Kienast, M., McCave, I. N., Lochte, A. A., Saini, J., Stein, R. & Hebbeln, D. 2021: Atlantic water inflow to Labrador Sea and its interaction with ice sheet dynamics during the Holocene. *Quaternary Science Reviews 256*, 106833, https://doi.org/10.1016/j.quascirev.2021.106833.

Werner, K., Mullner, J., Husum, K., Spielhagen, R. F., Kandiano, E. S. & Polyak, L. 2016: Holocene sea subsurface and surface water masses in the Fram Strait - comparisons of temperature and sea-ice reconstructions. *Quaternary Science Reviews 147*, 194–209.

Willemse, N. W. & Tornqvist, T. E. 1999: Holocene century-scale temperature variability from West Greenland lake records. *Geology 27*, 580–584.

Yunda-Guarin, G., Brown, T. A., Michel, L. N., Saint-Béat, B., Amiraux, R., Nozais, C. & Archambault, P. 2020: Reliance of deep-sea benthic macrofauna on ice-derived organic matter highlighted by multiple trophic markers during spring in Baffin Bay, Canadian Arctic. *Elementa: Science of the Anthropocene 8*, 047, https://doi.org/10.1525/elementa.2020.047.

Supporting Information

Additional Supporting Information to this article is available at http://www.boreas.dk.

Fig. S1. Comparison of GeoB19927-3 age-model determined by BACON (Saini *et al*. 2020) with the updated version using PDV (Langner & Mulitza 2019), which uses modelled reservoir ages (Butzin *et al*. 2017) and BACON. Note, the updated age-model (shown in brown) used in this study is about 0.2 ka younger than previously shown by Saini *et al*. (2020).

Fig. S2. Down-core variations of core GeoB19927-3 based on Saini *et al*. (2020): (a) bulk accumulation rate, and accumulation rates of (b) total organic carbon, (c) $CaCO_3$ (this study), (d) Z-HBI III, (e) dinosterol, (f) brassicasterol, and (g) sea-ice proxy IP_{25}. The orange box marks the ice-edge (IE) positions. All plots are shown vs. age in 1000 years before present (ka BP).

Fig. S3. Combined record of core GeoB19948-3: (a) $CaCO_3$ content, (b) total organic carbon (TOC), (c) HBI III (μg/g), (d) dinosterol (μg/g), (e) brassicasterol (μg/g), and (f) sea-ice proxy IP_{25}.

Fig. S4. Combined record of core GeoB19905-1: (a) $CaCO_3$ content, (b) total organic carbon (TOC), (c) dinosterol (μg/g), (d) brassicasterol (μg/g), and (e) sea-ice proxy IP_{25}.